
BACHELOR THESIS IN PHYSICS

THE SMUON AS THE LIGHTEST
SUPERSYMMETRIC PARTICLE IN R-PARITY
VIOLATING SUPERSYMMETRY

Written by
MARKUS RADZIEJ

Submitted to the
FACULTY FOR MATHEMATICS, COMPUTER SCIENCE AND
NATURAL SCIENCES

Created at the
III PHYS. INST. A
of the
RWTH AACHEN UNIVERSITY

Supervised by
PROF. DR. THOMAS HEBBEKER

July 27, 2011

I assure that I have created this document independently, have not used any sources or aids other than the ones I have listed and have labeled quotes as such.

Aachen the

Signature

Abstract

This thesis has its focal point on the possibilities of a smuon $\tilde{\mu}$ as a lightest supersymmetric particle in R-parity violating supersymmetry. The parameter space of the minimal supergravity model as well as the relevant λ couplings will be discussed. The goal is to illuminate the necessary relations between the parameters of the model, which allow for the $\tilde{\mu}$ as the lightest particle in the supersymmetric mass hierarchy. A chosen point in this parameter space will also be studied further by analyzing simulated proton-proton collisions at the current LHC center-of-mass energy of $\sqrt{s} = 7$ TeV.

Kurzfassung

Diese Bachelorarbeit befasst sich mit dem Stauon $\tilde{\mu}$ als leichtestes supersymmetrisches Teilchen in R-Paritäts verletzender Supersymmetrie. Sowohl der Phasenraum des Minimal Supergravity Models, als auch die relevante λ -Kopplung werden untersucht. Das Ziel der Arbeit ist es, die notwendigen Verhältnisse zwischen den Parametern des genannten Models zu bestimmen, welche es dem $\tilde{\mu}$ ermöglichen das Teilchen mit der geringsten Masse der supersymmetrischen Massenhierarchie zu sein. Ein konkreter Punkt des Phasenraums wird zudem noch untersucht, indem simulierte Proton-Proton Kollisionen bei der momentanen Schwerpunktsenergie von $\sqrt{s} = 7 \text{ TeV}$ analysiert werden.

Contents

1	Theoretical background	1
1.1	Standard model of particle physics	1
1.2	Supersymmetry	3
1.2.1	Minimal supersymmetric standard model	4
1.2.2	Minimal supergravity	5
1.3	Model specifications	6
1.3.1	Evolution of the righthanded smuon mass	8
1.3.2	Boundaries	9
2	Analysis	15
2.1	Scan of the parameter space	15
2.2	Basic analysis of a point in the parameter space	26
2.3	Conclusion	38
2.4	Acknowledgements	45

Chapter 1

Theoretical background

In this thesis all data is given in natural units, meaning that $\hbar = c = 1$. Energy is measured in eV, which is by definition the amount of kinetic energy gained by an electron when it accelerates through an electric potential difference of 1V. Thus one electronvolt equals $1.60217653(14) \cdot 10^{-19}$ J [1]. As a result of this choice of the system of units, the energy of a particle is given by $E^2 = m^2c^4 + p^2c^2 \Leftrightarrow E^2 = m^2 + p^2$.

1.1 Standard model of particle physics

The standard model of particle physics [2, 3, 4, 5] has been developed within the 20th century and its current formulation has been finalized in the 1970s. It describes, quite successfully, three of the four known interactions: Electromagnetism as well as the strong and weak interactions. Multiple particles, whose existence has been predicted by the standard model, have been discovered and have given credence to the theory. One can describe it as the basis of particle physics up to date.

According to the standard model, all matter is made of leptons and quarks. All particles are also split into fermions and bosons, with the fermions having an half-integer spin value and the bosons an integer spin value. The 12 fundamental leptons and quarks are split into three generations, sorted by mass (Fig. 1.1). Throughout each generation there are particles that are identical to each other, except for their higher mass in higher generations. All six quarks, marked in purple, are fermions having a spin value of 1/2. Their electric charge is either $2/3e$ for up-type quarks or $-1/3e$ for down type quarks. The leptons, marked in green, also consist of fermions with a spin value of 1/2. The electron-type fermions have a negative electric charge of $e = 1.602176487(40) \cdot 10^{-19}$ C [1], while the neutrinos do not have any

Three Generations
of Matter (Fermions)

	I	II	III	
mass→	2.4 MeV	1.27 GeV	171.2 GeV	0
charge→	$\frac{2}{3}$	$\frac{2}{3}$	$\frac{2}{3}$	0
spin→	$\frac{1}{2}$	$\frac{1}{2}$	$\frac{1}{2}$	1
name→	u up	c charm	t top	γ photon
Quarks	4.8 MeV $-\frac{1}{3}$ $\frac{1}{2}$ d down	104 MeV $-\frac{1}{3}$ $\frac{1}{2}$ s strange	4.2 GeV $-\frac{1}{3}$ $\frac{1}{2}$ b bottom	0 0 1 g gluon
	<2.2 eV 0 $\frac{1}{2}$ ν_e electron neutrino	<0.17 MeV 0 $\frac{1}{2}$ ν_μ muon neutrino	<15.5 MeV 0 $\frac{1}{2}$ ν_τ tau neutrino	91.2 GeV 0 1 Z⁰ weak force
	0.511 MeV -1 $\frac{1}{2}$ e electron	105.7 MeV -1 $\frac{1}{2}$ μ muon	1.777 GeV -1 $\frac{1}{2}$ τ tau	80.4 GeV ± 1 1 W[±] weak force
Leptons				Bosons (Forces)

Figure 1.1: Fundamental particles [6]

electric charge. Most particles have an antimatter equivalent, which have the negative value of the electric charge of their matter counterpart.

The gauge bosons, marked in red, have a spin value of 1. They act as carriers of the corresponding forces. The field theory used to describe the electromagnetic interaction is the quantum electrodynamics (QED). Its gauge boson is the photon γ , which couples to all particles with an electric charge. The weak interaction couples to all known fermions, but differently to righthanded and lefthanded ones. This parity violation is more distinct in the charged current interactions, transmitted by the W^\pm -bosons, than in the neutral current interactions of the Z -bosons. While the weak interaction is the only one that violates the parity-symmetry it is as well the only one that violates CP-symmetry. Aside from these violations, the weak interaction is exclusively able to change quark flavors. The mathematical model to describe the electromagnetic and weak interactions, the electroweak interactions is the quantum flavordynamics (QFD). This unification is mathematically achieved under an $SU(2) \times U(1)$ gauge group. The quantum chromodynamics (QCD) describe the strong interaction in the $SU(3)$ gauge group. In this model quarks and gluons have color charges, red, blue and green as well as their

anticolor counterparts. Quarks always couple together to a colorless particle. A particle consisting of 3 quarks, one of each color (or anticolor), is called a hadron. If a particle is made up of 2 quarks, one with a color and the other with the anticolor, it is a meson. As gluons carry color charges themselves, they couple to quarks as well as to other gluons. Even though in the quantum field theory (QFT) all gauge bosons are massless, there have been measurements of W^\pm and Z masses, which weigh 80.4 GeV and 91.2 GeV respectively. This phenomenon is described by the Higgs mechanism and its Higgs boson H , which allows those gauge bosons to have non vanishing masses through spontaneous symmetry breaking. Even though there is compelling evidence for the existence of the Higgs boson, the researchers of the Fermilab at the Tevatron and the LHC collaborations of CERN have yet to find this particle.

Though widely accepted and successful in its predictions, the standard model has a few drawbacks. For example physics of general relativity, such as dark matter or gravitation are not described by it. Also there is no candidate particle for the dark matter, which is (at least by the current understanding of interactions) required to exist due to mass insufficiencies in large galaxies, which would otherwise disperse. Another issue is the hierarchy problem of the Higgs mechanism, which poses the question, generally spoken, as to why the weak force is approximately 10^{32} times stronger than gravity. While these are not all noteworthy issues of the standard model one can see why, as a result of the multitude of unanswered questions, new theories have been developed and studied to provide possible answers.

1.2 Supersymmetry

The following paragraph and subsections are based on the references [7, 8, 9, 10]. One of the best studied theories beyond the standard model up to date is supersymmetry, often called SUSY. . In this theory each particle has a superpartner, which spin differs by half a unit, effectively relating each fermion to a boson and vice versa. If this symmetry should be realized in nature, it has to be broken, as there have been no superpartners observed, which means that their masses have to be significantly higher than those of common particles. Supersymmetry could solve the issues mentioned in the previous paragraph, having valid candidates for dark matter and allowing gravity to be incorporated into the theory of supersymmetry, which is then called supergravity. If supersymmetry exists at the TeV scale, it is also possible to solve the hierarchy problem with, for example, the minimal supersymmetric model [11]. The quantum corrections of the Higgs boson

mass, which beforehand pose a problem due to the magnitude, would be automatically canceled by its superpartner.

1.2.1 Minimal supersymmetric standard model

The minimal supersymmetric standard model, often abbreviated as MSSM, adds the minimal amount of superpartners necessary, which can be seen in Table 1.1. The nomenclature for this new set of particles adds an “s” at the front of each fermion superpartner (an electron becomes a selectron) and lets boson superpartners end in an “-ino” (meaning that a gluon becomes a gluino). Therefore one can already obtain basic information about the particle in question, just by hearing it’s name. The model itself is compatible with all current results from experiments, which is one of the reasons as to why it is called the standard model.

Standard model			Supersymmetric extension			
Particles	Spin	P_R	Gauge Eigenstate	Mass Eigenstate	Spin	P_R
Quarks			Squarks			
u d	1/2	+1	\tilde{u}_R \tilde{u}_L \tilde{d}_R \tilde{d}_L	\tilde{u}_R \tilde{u}_L \tilde{d}_R \tilde{d}_L	0	-1
s c	1/2	+1	\tilde{s}_R \tilde{s}_L \tilde{c}_R \tilde{c}_L	\tilde{s}_R \tilde{s}_L \tilde{c}_R \tilde{c}_L	0	-1
t b	1/2	+1	\tilde{t}_R \tilde{t}_L \tilde{b}_R \tilde{b}_L	\tilde{t}_1 \tilde{t}_2 \tilde{s}_1 \tilde{s}_2	0	-1
Leptons			Sleptons			
e ν_e	1/2	+1	\tilde{e}_R \tilde{e}_L $\tilde{\nu}_e$	\tilde{e}_R \tilde{e}_L $\tilde{\nu}_e$	0	-1
μ ν_μ	1/2	+1	$\tilde{\mu}_R$ $\tilde{\mu}_L$ $\tilde{\nu}_\mu$	$\tilde{\mu}_R$ $\tilde{\mu}_L$ $\tilde{\nu}_\mu$	0	-1
τ ν_τ	1/2	+1	$\tilde{\tau}_R$ $\tilde{\tau}_L$ $\tilde{\nu}_\tau$	$\tilde{\tau}_1$ $\tilde{\tau}_2$ $\tilde{\nu}_\tau$	0	-1
Neutral bosons			Neutralinos			
γ Z h H A	1, 0	+1	\tilde{B}^0 \tilde{W}^0 \tilde{H}_u^0 \tilde{H}_d^0	$\tilde{\chi}_1^0$ $\tilde{\chi}_2^0$ $\tilde{\chi}_3^0$ $\tilde{\chi}_4^0$	1/2	-1
Charged bosons			Charginos			
W^\pm H^\pm	1, 0	+1	\tilde{W}^\pm \tilde{H}_u^\pm \tilde{H}_d^\pm	$\tilde{\chi}_1^\pm$ $\tilde{\chi}_2^\pm$	1/2	-1
Gluon			Gluino			
g	1	+1	\tilde{g}	\tilde{g}	1/2	-1

Table 1.1: Here the MSSM superpartners as well as their standard model counterparts are displayed with some of their attributes. In particular the R-parity values P_R assigned to the particles are shown.

In table 1.1 one can see that the chirality of a supersymmetric particle matters significantly more than in the standard model. It results in an observable discrepancy between left- and righthanded masses. There is also a column which assigns the particles the R-parity P_R quantum number. It is calculated by $P_R = (-1)^{3B+L+2S}$, where B is the baryon number, L the lepton

number and S stands for the spin. A conserved R-parity quantum number allows for a LSP, short for lightest supersymmetric particle, to be stable, as this particular particle does therefore not decay any further because it is already the lightest of its R-parity quantum number. More importantly though, the proton can decay with a fairly short lifetime without imposing the conservation of P_R [12, 13, 14] or a local symmetry e.g. proton-hexality (P_6), because renormalizable lepton and baryon number violating interactions are possible. Both R-parity and proton-hexality prevent all lepton and baryon number violating interactions [15, 16, 17]. In case there are righthanded as well as lefthanded versions of a particle, the one in question for being the LSP usually is the righthanded one, because it is lighter than its counterpart. The LSP could potentially provide a candidate for the aforementioned dark matter. Usually the lightest neutralino $\tilde{\chi}_1^0$ is the particle of choice for the LSP as it is neutral, meaning that it is hard to detect because it does not take part in the electromagnetic interaction and therefore does not emit light.

Given supersymmetry, it is possible to unify all known interactions, which has been done in the ‘‘Grand unified theory’’, also known as GUT.

1.2.2 Minimal supergravity

Supergravity itself combines supersymmetry and general relativity. It follows naturally from supersymmetry due to the convolution of the Poincaré group [18]. The model with the minimal amount of supersymmetry charges ($N = 1$) is called ‘‘minimal supergravity’’, often abbreviated as mSUGRA. It is one of the most widely studied models of supergravity, which is also due to the low amount of parameters it requires to make predictions in comparison to the more than 100 free parameters in the MSSM. The five necessary parameters are the following ones [19, 20].

- m_0 is the universal scalar mass at the GUT scale M_{GUT} ($\mathcal{O}(10^{16})$)
- $m_{1/2}$ is the universal gaugino mass at the GUT scale M_{GUT}
- A_0 is the universal trilinear scalar coupling strength
- $\tan \beta$ denotes the tangents of the ratio of the two Higgs vacuum expectation values
- $\text{sgn } \mu$ describes the sign of the bilinear Higgs mixing parameter μ

To get from M_{GUT} to the electroweak scale, one uses the renormalization group equations (RGEs) to calculate the evolution of masses. Figure 1.2

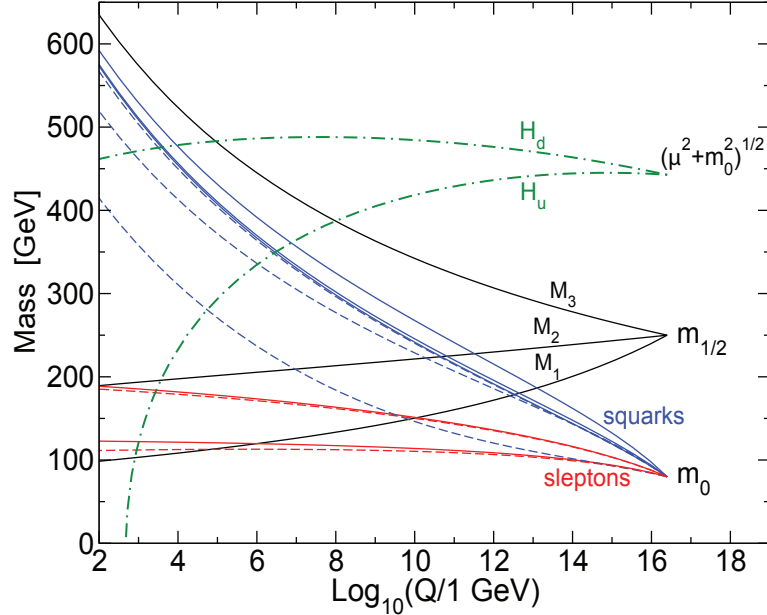


Figure 1.2: Mass evolution through RGEs, starting at M_{GUT} [10]. This gives an impression of how the parameters m_0 and $m_{1/2}$ have an impact on the mass spectrum.

provides an illustration of the importance regarding m_0 and $m_{1/2}$ in the evolution. One can see that the indices of the parameters indicate which particle masses they mainly influence, by referring to their spin. Therefore squarks and sleptons evolve from m_0 and M_1 , M_2 as well as M_3 which mix into the bosinos, root from $m_{1/2}$. One can already conclude that these are the main parameters that determine the mass spectrum of specific points in the parameter space. These have also been studied extensively in regards to the assumed future capabilities of the LHC.

1.3 Model specifications

This section will cover the specifics of the model, which will be used to analyze the supersymmetric mass spectrum. This is strongly inspired by H. K. Dreiner's publication [21].

One of the most interesting SUSY signatures, are multi-lepton final states [22, 23, 24]. The particles are fairly easy to identify and the background originating from the standard model is low. The LSP in this case, is supposed to decay into such states via lepton number violating (LNV) interactions.

The $\tilde{\mu}_R$ production is also relevant due to further theses being written by our institute, which also concern themselves with this particular particle and its cascades. Another aspect about the $\tilde{\mu}_R$ -LSP that makes it worth looking into, is the production of soft leptons. This means that the transversal momentum of the leptons is around 10 GeV and lower. One has to be aware of these kind of signatures because the triggers of the CMS detector have a fairly high threshold, which might cut out those leptons.

To achieve a $\tilde{\mu}_R$ LSP without allowing the proton to decay, a baryon-triality (B_3) discrete symmetry has been chosen [15, 16, 17, 25]. This local gauge symmetry alters the wave function for the chiral superfields:

$$\begin{aligned} \{Q^i\} &\rightarrow \{Q^i\} \\ \{H^U, \overline{D}^i\} &\rightarrow e^{2\pi i/3} \{H^U, \overline{D}^i\} \\ \{H^D, \overline{U}^i, L^i, \overline{E}^i\} &\rightarrow e^{4\pi i/3} \{H^D, \overline{U}^i, L^i, \overline{E}^i\} \end{aligned} \quad (1.1)$$

To reduce the relations 1.1 to just a single one, a coefficient α_j is introduced.

$$\psi_j \rightarrow e^{\alpha_j 2\pi i/3} \psi_j \quad (1.2)$$

α_j is assigned the values of table 1.2.

	Q^i	\overline{U}^i	\overline{D}^i	L^i	\overline{E}^i	H^D	H^U
α_j	0	2	1	2	2	2	1

Table 1.2: Assignment of the values of α_j to the respective superfield

The model allows for lepton number violating interactions, but not for baryon number violating ones. Large lepton number violating interactions at the grand unification scale reduce the mass of the smuon at the electroweak scale via the RGEs. The extension to the B_3 mSUGRA superpotential by lepton number violating terms is given by [26]:

$$W_{LNV} = \frac{1}{2} \lambda_{ijk} L_i L_j \overline{E}_k + \lambda'_{ijk} L_i Q_j \overline{D}_k + \kappa_i L_i H_2 \quad (1.3)$$

In the MSSM superpotential with R-parity conservation, these terms are absent. L_i and Q_i are the lepton and quark $SU(2)$ doublet superfields, whereas H_2 is the Higgs $SU(2)$ superfield that couples to the up-type quarks. \overline{E}_i and \overline{D}_i denote the lepton and down-type quark $SU(2)$ singlet superfields. The indices $i, j, k \in \{1, 2, 3\}$ refer to the particle generations. While the first coupling constant λ_{ijk} is antisymmetric in i and j and therefore only allows

for 9 couplings, λ'_{ijk} allows for 27 different couplings. κ_i denotes the bilinear coupling constants, which are three dimensional parameters that vanish in B_3 mSUGRA at M_{GUT} [19]. Only one of the remaining 36 couplings is assumed to be different from, and larger than 0 for this model. All values of λ_{ijk} are always given at the GUT scale for this research, which has been emphasized by the ‘‘GUT’’ addition next to the generation indices later on. If one provides a single coupling at the GUT scale, other couplings that violate the same lepton number are generated at the weak scale M_Z through the RGEs [19, 27, 28, 29].

1.3.1 Evolution of the righthanded smuon mass

To comprehend the dependence of the $\tilde{\mu}_R$ -mass at M_Z on the bounds at the GUT scale, one has to look at the relevant RGEs. These are modified by the LNV terms. The dominant contributions to the mass of the $\tilde{\mu}_R$ are given by the following equation [19].

$$16\pi^2 \frac{d(M_{\tilde{\mu}_R}^2)}{dt} = -\frac{24}{5}g_1^2|M_1|^2 + \frac{6}{5}g_1^2\mathcal{S} + 2(\mathbf{h}_{\mathbf{E}^k})_{ij}^2 + 4\lambda_{ijk}^2[(\mathbf{m}_{\tilde{\mathbf{Q}}}^2)_{ii} + (\mathbf{m}_{\tilde{\mathbf{L}}}^2)_{jj} + (\mathbf{m}_{\tilde{\mathbf{E}}}^2)_{kk}] \quad (1.4)$$

with

$$\mathcal{S} = \text{Tr}[\mathbf{m}_{\tilde{\mathbf{Q}}}^2 - \mathbf{m}_{\tilde{\mathbf{L}}}^2 - \mathbf{m}_{\tilde{\mathbf{U}}}^2 + \mathbf{m}_{\tilde{\mathbf{D}}}^2 + \mathbf{m}_{\tilde{\mathbf{E}}}^2] + m_{H_2}^2 - m_{H_1}^2 \quad (1.5)$$

as well as

$$(\mathbf{h}_{\mathbf{E}^k})_{ij} \equiv \lambda_{ijk} \cdot A_0 \text{ at } M_{\text{GUT}} \quad (1.6)$$

Here k is always 2 as the $\tilde{\mu}_R$ is the particle that is being discussed. g_1 is the $U(1)$ gauge coupling, with M_1 as the gaugino mass and $t = \ln Q$, where Q is the renormalization scale. The trilinear scalar soft breaking coupling $(\mathbf{h}_{\mathbf{E}^k})_{ij}$ is always related to λ_{ijk} as given by the equation 1.6.

The soft mass parameters in the last two equations (1.5 & 1.6), written in bold, are 3×3 matrices in flavor space. Here $\mathbf{m}_{\tilde{\mathbf{Q}}}$ and $\mathbf{m}_{\tilde{\mathbf{L}}}$ stand for the left-handed doublet squarks and sleptons, while the remaining $\mathbf{m}_{\tilde{\mathbf{U}}}$, $\mathbf{m}_{\tilde{\mathbf{D}}}$ and $\mathbf{m}_{\tilde{\mathbf{E}}}$ represent the respective singlet up-squarks, down-squarks and sleptons. The last terms, $m_{H_1}^2$ and $m_{H_2}^2$, are the scalar Higgs softbreaking masses.

In equation 1.4 the first two terms which are both proportional to the gauge coupling g_1^2 , are *negative* at any scale. In particular the term proportional to \mathcal{S} becomes identical to zero at the GUT scale due to universal

scalar masses. Their contribution to the mass of the smuon $M_{\tilde{\mu}_R}^{k=2}$ will therefore *increase* the value when running from M_{GUT} to M_Z . While these terms are also present in P_R conserving models, the latter ones are not. The latter ones are proportional to λ_{ijk}^2 and $(\mathbf{h}_{\mathbf{E}^k})_{ij}^2$, which means they are also proportional to λ_{ijk}^2 as explained beforehand. Their contribution is entirely *positive* and therefore *decreases* $M_{\tilde{\mu}_R}$ as it runs from M_{GUT} towards M_Z . The order of magnitude of the LNV coupling λ_{ijk} has to be similar to the one of the gauge coupling g_1 ($\mathcal{O}(10^{-2})$) to be able to reduce the mass of the smuon significantly enough for it to be the LSP. On account of the dependence of the smuon mass on the coupling itself, it becomes another addition to the parameters of the B_3 mSUGRA model that has to be taken into account when searching for the smuon as the LSP.

1.3.2 Boundaries

The boundaries of the respective parameters have to be taken into consideration as well, when researching the parameter space which allows for a smuon LSP. While the B_3 mSUGRA model does not pose any hard restraints on the parameters, certain sections of the parameter space can already be excluded with the results from particle accelerators such as the LEP or the LHC.

The universal scalar and gaugino masses m_0 and $m_{1/2}$ m_0 and $m_{1/2}$ are the most commonly studied parameters, as their ratio determines the general mass spectrum. Figure 1.3 shows the estimated possibilities of masses of gluinos in the m_0 against $m_{1/2}$ space the LHC is able to reach after further development on its current status. After 3 years the LHC should be able to produce gluinos with a mass of 3 TeV. This corresponds to a $m_{1/2}$ of roughly 1400 TeV. As mentioned before, this does not pose a hard upper limit for $m_{1/2}$, but gives an idea of where of the experimental limitation with the LHC. Thus values of $m_{1/2}$ which are larger than 1400 TeV are not taken into consideration for this analysis. The upper bound for m_0 is strictly related to the value of $m_{1/2}$ and depends on the region where the $\tilde{\mu}_R$ remains a candidate for the LSP. Figure 1.3 shows an upper limit of around 600 GeV for $m_{1/2} = 1400$ GeV, where charged LSPs are still possible. The necessary ratio of m_0 to $m_{1/2}$ will be studied in the “scan of the parameter space” section (Sec. 2.1). Regarding the lower limits, figure 1.3 shows that $m_{1/2}$ is bound at 150 GeV by chargino searches at the LEP accelerator. For m_0 the lower bound is given by a charged particle becoming the LSP, which is not the common scenario for the MSSM searches. For the particular case that is being studied here, this does not apply and therefore m_0 is allowed to be reduced even further.

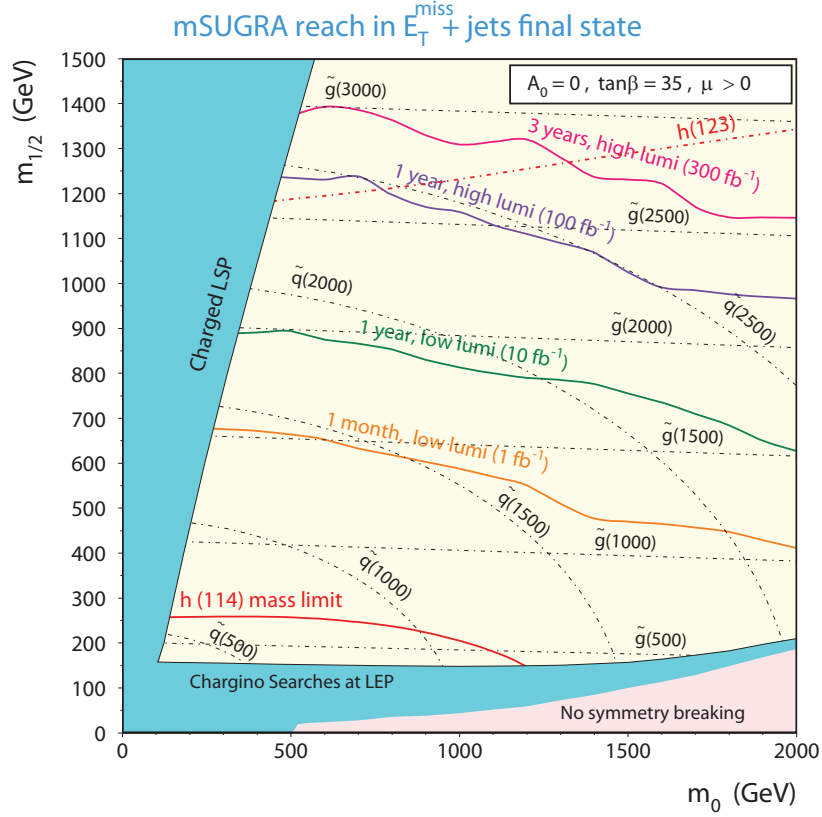


Figure 1.3: Longterm reach of the LHC in the mSUGRA model at $\sqrt{s} = 14$ TeV [30]

The trilinear coupling A_0 A_0 enters the equation for the slepton mass (1.4) via the LNV soft-breaking trilinear scalar coupling $(\mathbf{h}_{\mathbf{E}_k})_{ij}$ (1.6). As $t = \ln Q$ decreases, $(\mathbf{h}_{\mathbf{E}_k})_{ij}$ contributes to $M_{\tilde{l}_R=2}$ through the integral over t from the electroweak scale $t_Z = \ln M_Z$ to the GUT scale $t_{\text{GUT}} = \ln M_{\text{GUT}}$. The difference between the runnings of A_0 for different signs can be comprehended, by examining the RGE of $(\mathbf{h}_{\mathbf{E}_k})_{ij}$ [19].

$$16\pi^2 \frac{d(\mathbf{h}_{\mathbf{E}_k})_{ij}}{dt} = -(\mathbf{h}_{\mathbf{E}_k})_{ij} \cdot \left(\frac{9}{5}g_1^2 + 3g_2^2 \right) + \lambda_{ijk} \cdot \left(\frac{18}{5}g_1^2 M_1 + 6g_2^2 M_2 \right) \quad (1.7)$$

As in Equation 1.4 g_i , $i \in \{1, 2\}$, are the gauge couplings and M_1 and M_2 denote the $U(1)$ and $SU(2)$ gaugino masses. The righthand side is divided into two terms which are proportional to $(\mathbf{h}_{\mathbf{E}_k})_{ij}$ and λ_{ijk} , respectively. Equation 1.6 shows that the sign of $(\mathbf{h}_{\mathbf{E}_k})_{ij}$ depends on the sign of A_0 , as λ_{ijk} is assumed to be positive or zero at all times. This means that a positive A_0 leads

to a *negative* first term on the righthand side of equation 1.7, which results in an increase of $(\mathbf{h}_{\mathbf{E}_k})_{ij}$ while running from M_{GUT} to M_Z . The second term proportional to λ_{ijk} is always positive and even though λ_{ijk} increases slightly, the gauge couplings g_i and gaugino masses M_i , $i \in \{1, 2\}$, decrease while lowering the scale. Thus the first term will become the dominant contribution towards lower scales. While a positive A_0 leads to a compensation of the terms respectively proportional to $(\mathbf{h}_{\mathbf{E}_k})_{ij}$ and λ_{ijk} , a negative A_0 leads to a *positive* first term. Both terms being positive leads to an overall increased $(\mathbf{h}_{\mathbf{E}_k})_{ij}$ as there is no more compensation. As a consequence only negative A_0 will be considered in the analysis, because they provide larger $(\mathbf{h}_{\mathbf{E}_k})_{ij}$ and therefore decrease $M_{\tilde{R}^{k=2}} = M_{\tilde{\mu}_R}$ as explained in the previous section (Sec. 1.3.1). As for the lower bound on A_0 , there is once again no hard limit for the value itself, but the LEP research has provided a lower limit on the lightest Higgs mass of 114.4 GeV [31, 32]. Because A_0 also enters the RGE of the mass of the lightest Higgs m_{h^0} , this does limit the allowed range of values for A_0 in dependence of the remaining parameters. This will be shown in the two dimensional histograms of section 2.1.

The tangents of the ratio of the two Higgs vacuum expectation values $\tan\beta$ $\tan\beta$ is also bound by results from the LEP experiment. While the lower bound is approximately 3.4 [33, 34], the upper bound for this scenario is given by the rapidly decreasing $\tilde{\tau}_1$ mass with a rising value of $\tan\beta$. The lower bound is also dependent on the sign of μ . The lower limit of 3.4 is for a positive sign of μ . A negative sign would lead to a higher value for the lower bound [33], which excludes almost the entire region relevant for this research, because any values higher than 10 can be neglected for the current LHC state as the “scan of the parameter space” section (Sec. 2.1) will show.

The LNV couplings λ_{ijk} λ_{ijk} has three permutations of i, j, k that may result in a $\tilde{\mu}_R$ -LSP. Of the three options for the LNV coupling, the restrictions on λ_{212} and λ_{232} are generally too strong to allow for the $\tilde{\mu}_R$ -LSP [19]. The remaining $\lambda_{132|_{\text{GUT}}}$ has the following upper bound 2σ limit.

$$\lambda_{132|_{\text{GUT}}} \lesssim 0.03 \cdot \left(\frac{M_{\tilde{\mu}_R}}{100 \text{ GeV}} \right) \quad (1.8)$$

This value has been calculated including the most recent bounds from the Babar Experiment of 2008 [35]. The calculation of the parameter limit has been done to a 95% confidence level. Starting with the branching fractions of muons and taus, which are shifted due to the $L_i L_j \bar{E}_k$ (1.3) term, the

equations for the corrections of the ratio of the branching fractions have the following form.

$$R_{\tau\mu} = [R_{\tau\mu}]_{SM} \cdot [1 + 2(r_{23k}(\tilde{e}_{kR}) - r_{12k}(\tilde{e}_{kR}))] \quad (1.9)$$

$$R_{\tau} = [R_{\tau}]_{SM} \cdot [1 + 2(r_{13k}(\tilde{e}_{kR}) - r_{23k}(\tilde{e}_{kR}))] \quad (1.10)$$

with the LNV coupling in

$$r_{ijk} = \frac{1}{4\sqrt{2}G_F} \frac{|\lambda_{ijk}|}{M_{\tilde{l}_R}^2} \quad (1.11)$$

as well as the standard model predictions of the decay width

$$R_{\tau\mu} = \frac{\Gamma(\tau \rightarrow \mu \bar{\nu}_{\mu} \nu_{\tau}(\gamma))_{SM}}{\Gamma(\mu \rightarrow e \bar{\nu}_e \nu_{\tau}(\gamma))_{SM}} = 1.312 \cdot 10^6 \quad (1.12)$$

$$R_{\tau} = \frac{\Gamma(\tau \rightarrow e \bar{\nu}_e \nu_{\tau}(\gamma))_{SM}}{\Gamma(\tau \rightarrow \mu \bar{\nu}_{\mu} \nu_{\tau}(\gamma))_{SM}} = 1.028 \quad (1.13)$$

$$(1.14)$$

and calculated average values for the branching fractions from the particle data group [36]

$$R_{\tau\mu} = \frac{\tau_{\mu}}{\tau_{\tau}} \mathcal{S}(\tau \rightarrow \mu \bar{\nu}_{\mu} \nu_{\tau}(\gamma)) = (1.312 \pm 0.006) \cdot 10^6 \quad (1.15)$$

$$R_{\tau} = \frac{\mathcal{S}(\tau \rightarrow e \bar{\nu}_e \nu_{\tau}(\gamma))}{\mathcal{S}(\tau \rightarrow \mu \bar{\nu}_{\mu} \nu_{\tau}(\gamma))} = 1.028 \pm 0.004 \quad (1.16)$$

$$(1.17)$$

Since only one of the couplings is supposed to be zero at a time, the equation for $\lambda_{132|GUT}$ becomes linear with only one unknown. To ensure a 95% confidence level, one adds 2σ to the measured mean and solves the equation for $\lambda_{132|GUT}$. Depending on value of R_{τ} the limit for $\lambda_{132|GUT}$ varies, meaning that taking the latest measurement from the Babar group into account as well, the limit gets lowered.

$$|\lambda_{132}| \cdot \left(\frac{100 \text{ GeV}}{M_{\tilde{l}_R}} \right) \approx \begin{cases} 0.05 & \text{for } R_{\tau} = 1.028 \pm 0.004 \\ 0.02 & \text{for } [R_{\tau}]_{\text{Babar08}} = 1.021 \pm 0.004 \\ 0.03 & \text{for avg. } R_{\tau} = 1.025 \pm 0.003 \end{cases} \quad (1.18)$$

Choosing the average value is the most plausible choice, since neither discarding years of research and relying on one measurement or disregarding new measurements is a reasonable approach. Note though, that the means of the old world avg. and the measurement from the Babar experiment do not fit well together, as they are not in 2σ range of each other. Due to this less than optimal fit, the calculated upper bound for the LNV coupling could also vary quite a lot because it is so sensitive to the value of R_τ .

Given these limits, one can scan the parameter space for the desired $\tilde{\mu}_R$ -LSP, which will be done in the following analysis chapter.

Chapter 2

Analysis

The analysis is divided into two sections. In the first section an somewhat iterative approach to scanning the parameter space will be presented, while in the second section there will be a basic analysis of a chosen point of the scanned parameter space. As for the application used to calculate the mass spectra, `SOFTSUSY 3.1.7` [37, 38] has been chosen. To provide the necessary data to generate events with `HERWIG 6.510` [39, 40] an additional application is required, as e.g. branching fractions are not calculated by `SOFTSUSY 3.1.7`. Because an interface for `ISAJET 7.64` [41] has already been implemented into `SOFTSUSY 3.1.7`, the software has been used to generate the inputfile for `HERWIG 6.510`. Note that `ISAJET 7.64` is not the latest version up to date, but at the time of writing the interface of `SOFTSUSY 3.1.7` is incompatible with newer versions.

2.1 Scan of the parameter space

Since there is no simple array of equations that provide comprehensive analytic solutions to the question where the $\tilde{\mu}_R$ is the LSP, a numeric/iterative approach has been chosen. To select a suitable starting point for this approach, one has to be aware of the basic evolution of masses depending on the relations between the parameters. These relations will be illustrated as a next step.

As discussed beforehand, a fairly large, negative A_0 has to be chosen. To reduce the mass splitting between the neutralino and slepton masses, the universal scalar mass m_0 has to be significantly higher than the universal gaugino mass $m_{1/2}$. $\tan\beta$ has a lower limit, but will quickly force a τ -LSP when chosen too high. The sign of the bilinear Higgs mixing parameter μ is positive, as it would raise the limit on $\tan\beta$ otherwise. In general the

starting point should be chosen with reasonably low values of m_0 and $m_{1/2}$ so a discovery of a similar scenario is possible with early LHC data. Note that all current CMS mSUGRA benchmark points [42] do not include configurations that allow for other sparticles than the lightest neutralino $\tilde{\chi}_1^0$ to be the LSP.

m_0 in GeV	$m_{1/2}$ in GeV	A_0 in GeV	$\tan \beta$	$\text{sgn } \mu$
100	550	-1500	4	+

Table 2.1: Starting point in the B_3 mSUGRA parameter space, inspired by H. K. Dreiner's publication [21]

Using the parameters given in Table 2.1, one can determine a reasonable value of $\lambda_{132|GUT}$ for further analysis of the parameter space. This is done by running over the LNV coupling while observing the masses of the lightest sparticles.

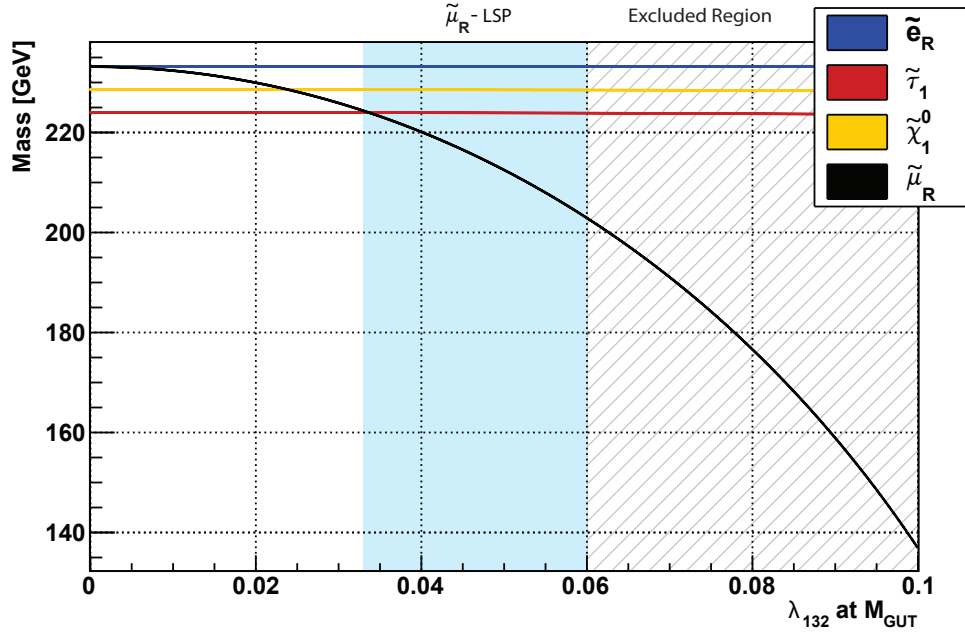


Figure 2.1: Sparticle masses as a function of $\lambda_{132|GUT}$ to determine the width of the $\tilde{\mu}_R$ -LSP space. The $\tilde{\mu}_R$ becomes the LSP at $\lambda_{132|GUT} = 0.034$, whereas the maximal allowed value of $\lambda_{132|GUT}$ is 0.061

The blue, highlighted part in Figure 2.1 marks the region where the $\tilde{\mu}_R$ has become the LSP, while $\lambda_{132|GUT}$ is within the experimentally allowed region. The values of $\lambda_{132|GUT}$, which exceed the bound are marked by the patterned region. Even with an intentionally chosen starting point, the width

of the $\tilde{\mu}_R$ -LSP region is quite small. To increase the extend of the blue area, either the $\tilde{\mu}_R$ has to become the LSP earlier, or the upper bound, which is dependent on the mass of the $\tilde{\mu}_R$, needs to be raised. To study the effect on the blue $\tilde{\mu}_R$ -LSP region of shifting the parameters in one direction, a single parameter will be varied while the remaining ones will be kept at the starting point values (Tab. 2.1).

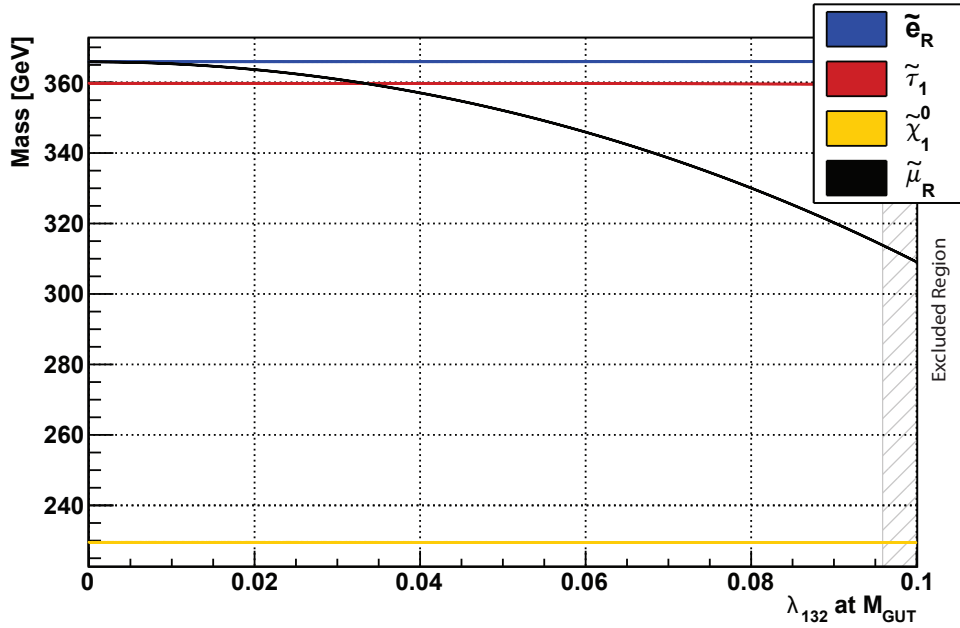


Figure 2.2: Sparticle masses as a function of $\lambda_{132|GUT}$ with an increased value of m_0 : $A_0 = -1500$ GeV, $\mathbf{m}_0 = 300$ GeV, $m_{1/2} = 550$ GeV, $\tan \beta = 4$, $\text{sgn } \mu = +$, $\lambda_{132|GUT} = 0.045$. No $\tilde{\mu}_R$ -LSP region for any $\lambda_{132|GUT}$ and maximal allowed value of $\lambda_{132|GUT} = 0.097$

For m_0 the result is fairly straight forward. Figure 2.2 shows the effect of increasing m_0 to 300 GeV. One can clearly see that, even though the evolution of the sfermion masses is similar to what has been shown in Figure 2.1, the lightest neutralino $\tilde{\chi}_1^0$ is almost not affected by the increase of m_0 , leading to a $\tilde{\chi}_1^0$ -LSP for all allowed values of $\lambda_{132|GUT}$. This result was to be expected with the information given in section 1.2.2, that m_0 is the main contribution to the sfermion masses and therefore has a major impact on their mass spectrum, but only little to none on the other mass spectra. Note how the upper limit on $\lambda_{132|GUT}$ has shifted towards a value of almost 0.1, due to the increase of the $\tilde{\mu}_R$ mass on which the bound depends. Even though the limit has risen significantly, there is still no $\tilde{\mu}_R$ -LSP region.

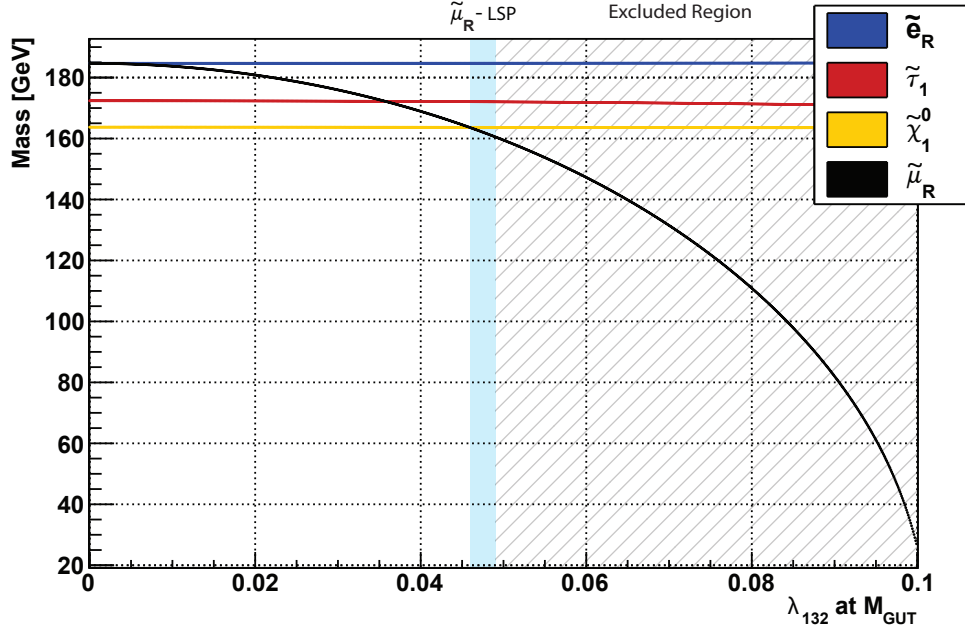


Figure 2.3: Sparticle masses as a function of $\lambda_{132|_{\text{GUT}}}$ with a decreased value of $m_{1/2}$: $A_0 = -1500 \text{ GeV}$, $m_0 = 100 \text{ GeV}$, $\mathbf{m}_{1/2} = 400 \text{ GeV}$, $\tan \beta = 4$, $\text{sgn } \mu = +$, $\lambda_{132|_{\text{GUT}}} = 0.045$. First $\tilde{\mu}_R$ -LSP at $\lambda_{132|_{\text{GUT}}} = 0.046$ and maximal allowed value of $\lambda_{132|_{\text{GUT}}} = 0.048$

Similarly to the increase of m_0 , reducing $m_{1/2}$ results in a $\tilde{\chi}_1^0$ -LSP for the most part. Note that in Figure 2.3 all masses are reduced, instead of just the sfermion masses for the m_0 variation (Fig. 2.2). $m_{1/2}$ is less of handle between gaugino and sfermion masses than m_0 , as it influences both mass spectra simultaneously. This means that $m_{1/2}$ is of even higher importance than m_0 when looking for the $\tilde{\mu}_R$ -LSP, as it effectively determines the range of the sparticle masses. The remaining region with a $\tilde{\mu}_R$ -LSP is very narrow and close to extinction as the bound on $\lambda_{132|_{\text{GUT}}}$ has been reduced as a consequence of the lower $\tilde{\mu}_R$ mass.

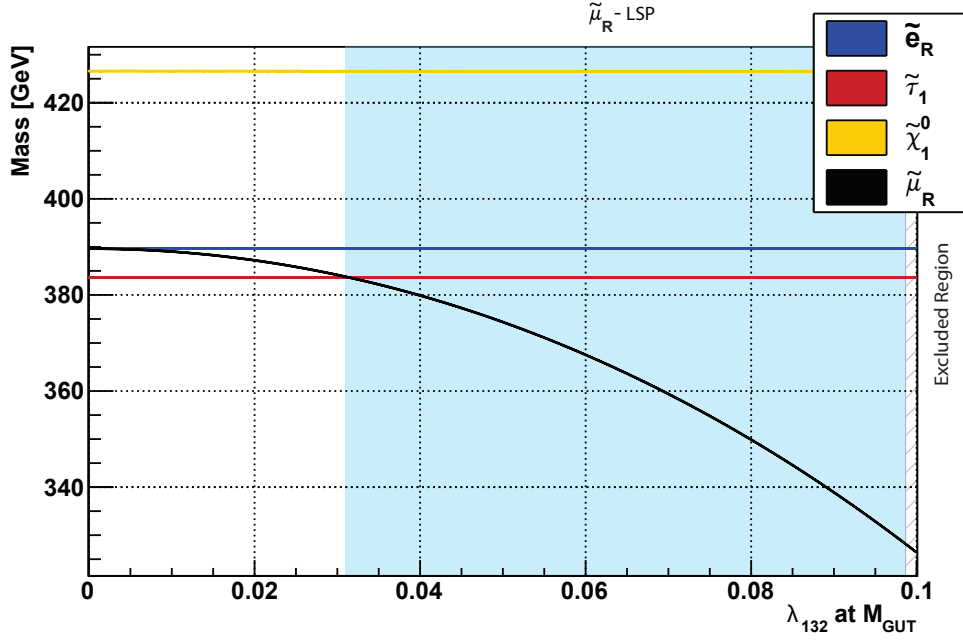


Figure 2.4: Sparticle masses as a function of $\lambda_{132|GUT}$ with an increased value of $m_{1/2}$: $A_0 = -1500$ GeV, $m_0 = 100$ GeV, $\mathbf{m}_{1/2} = 1000$ GeV, $\tan \beta = 4$, $\text{sgn } \mu = +$, $\lambda_{132|GUT} = 0.045$. First $\tilde{\mu}_R$ -LSP at $\lambda_{132|GUT} = 0.032$ and maximal allowed value of $\lambda_{132|GUT} = 0.099$

Increasing $m_{1/2}$ on the other hand will push the $\tilde{\chi}_1^0$ mass above the one of the $\tilde{\mu}_R$ and also the one of $\tilde{\tau}_1$ for even higher values. Figure 2.4 shows the $\tilde{\chi}_1^0$ constantly being the heaviest amongst the 4 shown particle masses, meaning that in comparison to figure 2.1, the $\tilde{\chi}_1^0$ does not determine the point at which $\tilde{\mu}_R$ becomes the LSP. The $\tilde{\tau}_1$ takes that role in this configuration of parameters. Similarly to the previous figure (Fig. 2.3), both the gaugino as well as the sfermion masses are affected by the increased value of $m_{1/2}$. Raising the sfermion masses also leads to a higher upper bound on $\lambda_{132|GUT}$, thus increasing the width of the $\tilde{\mu}_R$ -LSP region by quite a lot. Even though this configuration offers the widest $\tilde{\mu}_R$, centering the studies around this point is less favorable as the sparticle masses of the relevant decay channels leading to the $\tilde{\mu}_R$ are way too heavy to be found with the current state of the LHC.

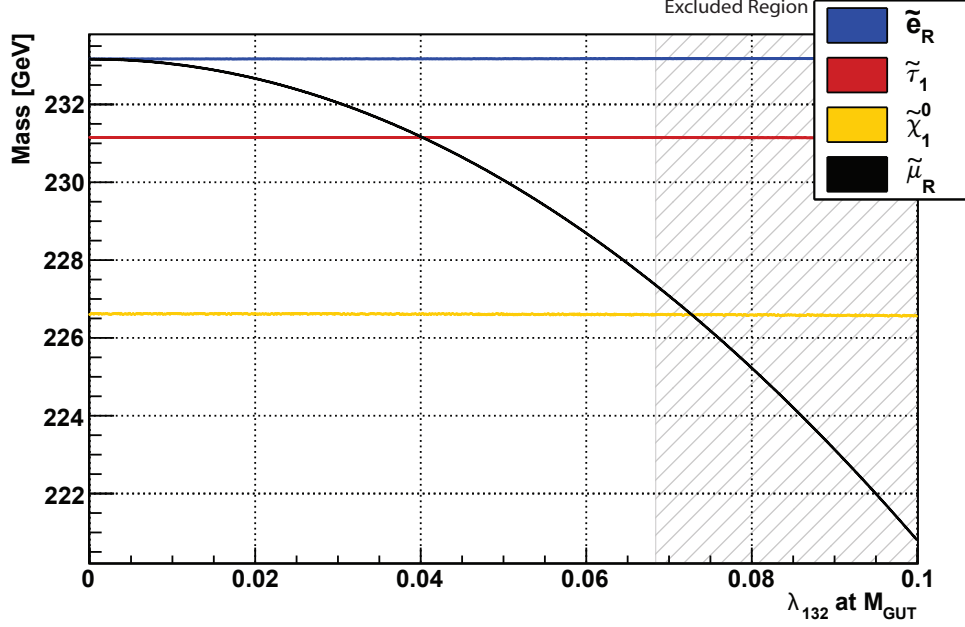


Figure 2.5: Sparticle masses as a function of $\lambda_{132|GUT}$ with an increased value of A_0 : $\mathbf{A}_0 = -300 \text{ GeV}$, $m_0 = 100 \text{ GeV}$, $m_{1/2} = 550 \text{ GeV}$, $\tan \beta = 4$, $\text{sgn } \mu = +$, $\lambda_{132|GUT} = 0.045$. No $\tilde{\mu}_R$ -LSP region for any $\lambda_{132|GUT}$ and maximal allowed value of $\lambda_{132|GUT} = 0.068$

The dependence on A_0 is not as straight forward as the previous two parameters. As explained in section 1.3.1, A_0 enters the equation for the $\tilde{\mu}_R$ through the trilinear scalar soft breaking coupling $(\mathbf{h}_{\mathbf{E}^k})_{ij}$. Thus the evolution of the $\tilde{\mu}_R$ -mass should be altered, when changing the value of A_0 . Note the small width of the mass scale, which is the result of the minimal reduction of the $\tilde{\mu}_R$ -mass over the running of $\lambda_{132|GUT}$. Large values of A_0 may lead to a root of the function for the $\tilde{\mu}_R$ mass. However this is irrelevant as the lowest allowed values for sparticle masses have already been researched and are listed in the publications of the particle data group [36]. For righthanded sleptons they are around 90 GeV to 110 GeV. Once again there is no $\tilde{\mu}$ -LSP for any value of $\lambda_{132|GUT}$ as the evolution of masses of the $\tilde{\mu}_R$ and the $\tilde{\chi}_1^0$ intersect in the excluded region. Compared to figure 2.2 the reduction of A_0 is of less importance than the increase of m_0 regarding the $\tilde{\mu}$ -LSP.

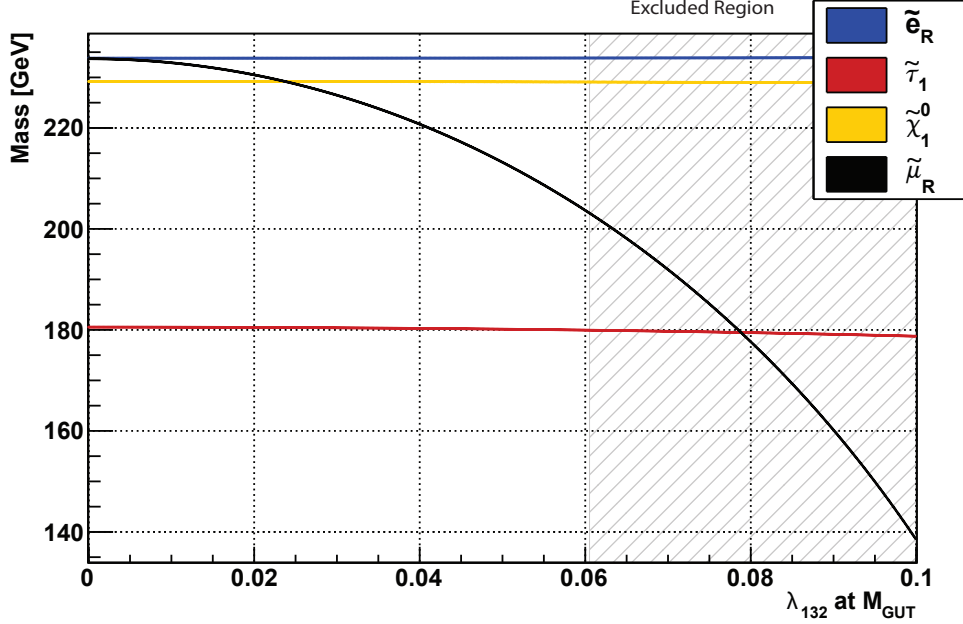


Figure 2.6: Sparticle masses as a function of $\lambda_{132|GUT}$ with an increased value of $\tan\beta$: $A_0 = -1500$ GeV, $m_0 = 100$ GeV, $m_{1/2} = 550$ GeV, $\tan\beta = 10$, $\text{sgn}\mu = +$, $\lambda_{132|GUT} = 0.045$. No $\tilde{\mu}_R$ -LSP region for any $\lambda_{132|GUT}$ and maximal allowed value of $\lambda_{132|GUT} = 0.061$

$\tan\beta$ does contribute to the $\tilde{\tau}_1$ mass, but not to the mass of the $\tilde{\mu}_R$. An increased value for $\tan\beta$ results in an increased τ Yukawa coupling, which leads to a higher *negative* contribution to the $\tilde{\tau}_1$ mass over the RGE running [43, 44]. Higher $\tan\beta$ also lead to a larger mixing of the $\tilde{\tau}_R$ and $\tilde{\tau}_L$. As one can see in figure 2.6, $\tan\beta$ drops the $\tilde{\tau}_1$ mass to the LSP level. The $\tilde{\mu}_R$ can only become the LSP at high values of $\lambda_{132|GUT}$, which are usually excluded by the bound on the LNV coupling. Similarly to the previous figure, the $\tilde{\mu}_R$ -LSP region appears to be almost in reach for this set of parameters. However as the ratio between the $\tilde{\tau}_1$ and the $\tilde{\mu}_R$ mass is affected, it is not possible for the $\tilde{\mu}_R$ to be the LSP without any drastic variation of the remaining parameters. Taking a look at the figure for the increased $m_{1/2}$ (Fig. 2.4), one can see that the upper bound of $\lambda_{132|GUT}$ can be extended towards 0.1. As the maximal allowed value for $m_{1/2}$ for research at the LHC is 1400 GeV, this means that $\tan\beta$ can be raised above 10 while still being within the experimentally allowed bound for $\lambda_{132|GUT}$. As the LHC cannot reach these high values for $m_{1/2}$ yet, our studies are more limited. The exact value for our upper bound on $\tan\beta$ will be given in figure 2.9 later on.

As a preliminary conclusion, one can already see that only certain ratios

between parameters are allowed, whereas too much deviation from those ratios leads to a different sparticle as the LSP. To actually determine the range in which the parameters still lead to the desired $\tilde{\mu}_R$ -LSP, the parameter space has to be scanned centering around a certain set of starting parameters. In order to do that, two dimensional histograms will be used to show the $\tilde{\mu}_R$ -LSP regions, while all other parameters will be kept constant.

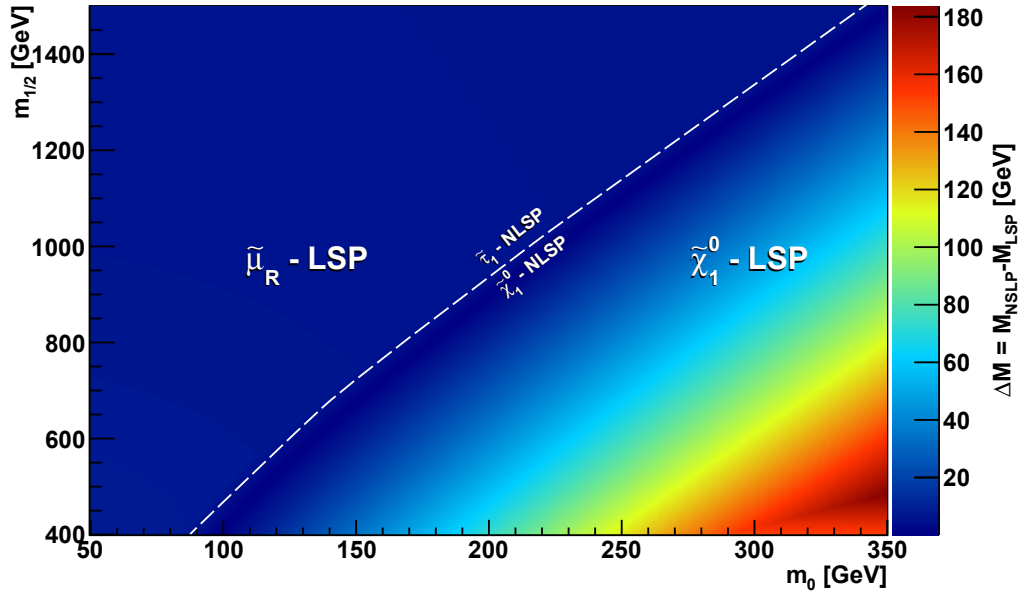


Figure 2.7: Plot of m_0 against $m_{1/2}$ with the following constant parameters:
 $A_0 = -1500$ GeV, $\tan \beta = 4$, $\text{sgn } \mu = +$, $\lambda_{132|GUT} = 0.045$.

To start off, m_0 will be plotted against $m_{1/2}$ to see in which area of figure 1.3 this scan operates. Anything below roughly 400 GeV for $m_{1/2}$ does not lead to a $\tilde{\mu}_R$ -LSP with the given set of parameters and is therefore not included in figure 2.7. On the other hand the upper limits for each parameter are the ones from section 1.3.2. As expected one can see that the shown $\tilde{\mu}_R$ -LSP region is restricted to the “charged LSP” region of figure 1.3. The color of each bin is dependent on the mass difference between the LSP and the next to LSP (NLSP), where the blue shades represent low differences and the red ones the high differences. The difference in the mass spectrum also rises significantly with a higher m_0 , because this parameter functions like a handle between gaugino and sfermion masses as shown in figure 2.2, whereas for lower m_0 for any value of $m_{1/2}$ the difference remains below 20 GeV. Note that the transition from the $\tilde{\mu}_R$ -LSP to the $\tilde{\chi}_1^0$ -LSP *does* come hand in hand

with an NLSP switch from the $\tilde{\chi}_1^0$ to the $\tilde{\mu}_R$. The region with this hierarchy is very small though, due to the $\tilde{\tau}_1$ mass being only slightly larger than the one of the $\tilde{\mu}_R$, which only allows a $\tilde{\chi}_1^0$ -NLSP for a 10 GeV range in m_0 . As a conclusion for this figure one can see that for this set of parameters the ratio of the values of $m_{1/2}$ to m_0 has to be higher than 4 to allow for an $\tilde{\mu}_R$ -LSP. For lower values of m_0 (around 130 GeV and less) the required ratio rises, though not linearly.

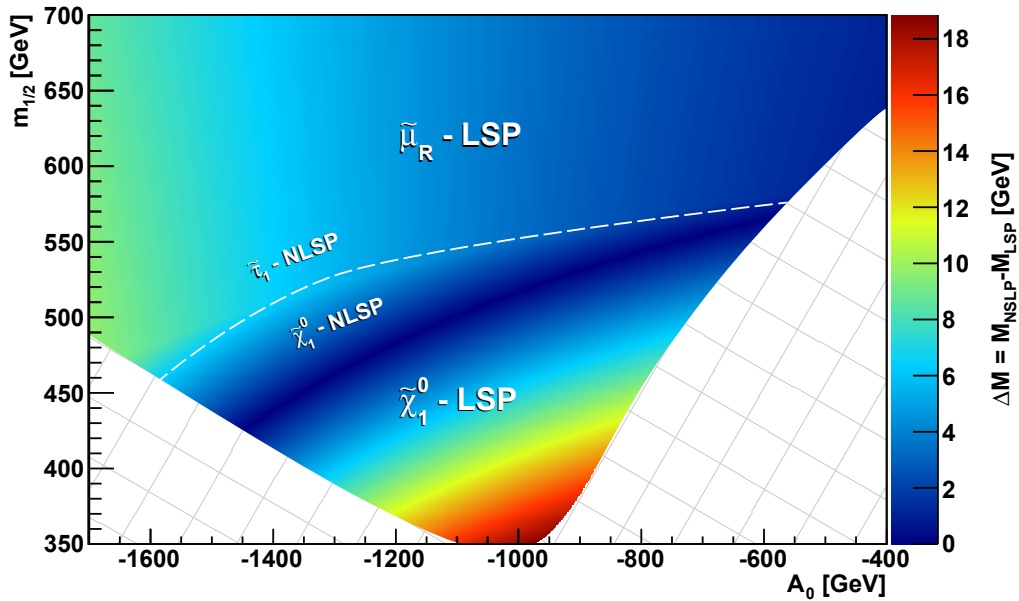


Figure 2.8: Plot of A_0 against $m_{1/2}$ with the following constant parameters: $m_0 = 100$ GeV, $\tan\beta = 4$, $\text{sgn}\mu = +$, $\lambda_{132|\text{GUT}} = 0.045$. The patterned region is excluded by LEP searches.

Another interesting plot is A_0 against $m_{1/2}$, as one of those parameters determine the basic shape of the mass spectrum, whereas the other one can shape the hierarchy in between the sparticle groups under the given circumstances. Figure 2.8 shows the border at which the trilinear coupling strength A_0 becomes high enough in regards to the $m_{1/2}$ value, to allow for a $\tilde{\mu}_R$ -LSP. The shown region is once again limited by the fact that there is no $\tilde{\mu}_R$ -LSP for lower values of $m_{1/2}$ or high values of A_0 . The color scheme is identical to the previous figure (Fig. 2.7). Note however, that the mass differences are very small overall. Their range extends only from 0 GeV to 20 GeV in comparison to the 0 GeV to 180 GeV scale of figure 2.7. The patterned region is excluded by the LEP limit on the lightest Higgs mass, as explained in section

1.3.2. However the limit has been reduced by 3 GeV to account for numerical uncertainties of SOFTSUSY 3.1.7 [45, 46, 47]. Here the switch of the LSPs does coincide with switch of the NLSPs for the $\tilde{\mu}_R$ to the lightest neutralino $\tilde{\chi}_1^0$ as the NLSP as well, but not for the transition from the $\tilde{\chi}_1^0$ to $\tilde{\tau}_1$ for which the additional dashed line has been added to show the transition. One can see that, as mentioned in section 1.3.2, only large values of A_0 in relation to $m_{1/2}$, lead to a $\tilde{\mu}_R$ -LSP.

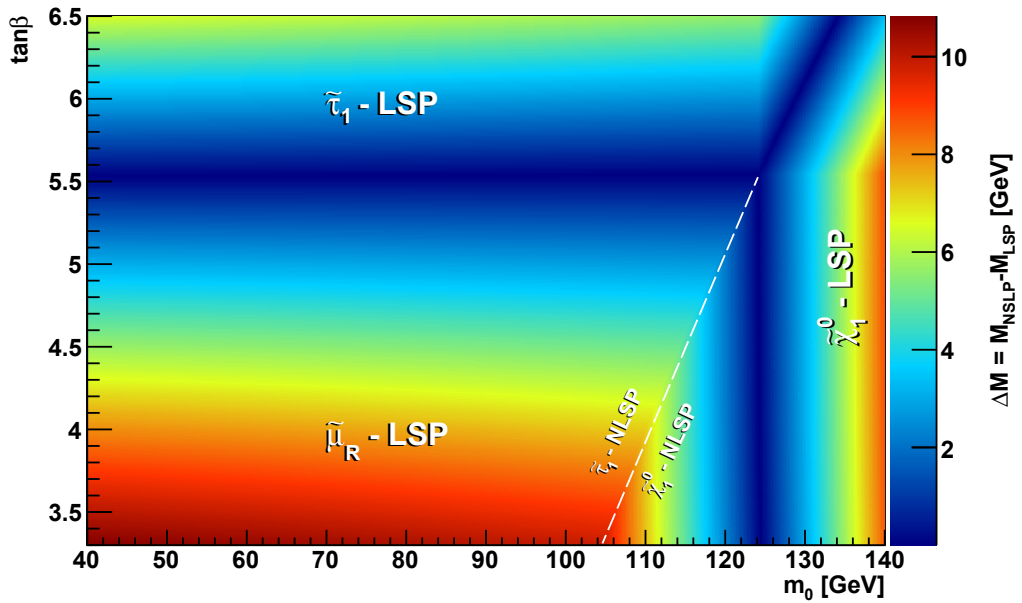


Figure 2.9: Plot of m_0 against $\tan\beta$ with the following constant parameters:
 $A_0 = -1500$ GeV, $m_{1/2} = 550$ GeV, $\text{sgn}\mu = +$, $\lambda_{132|\text{GUT}} = 0.045$.
 Values lower than 3.4 for $\tan\beta$ have been excluded by LEP searches.

The parameters that work as a handle are shown in figure 2.9. Both their bounds are dependent on the other parameters. Thus the range of both parameters is quite limited. A $\tan\beta$ of around 5.6 and higher leads to $\tilde{\tau}_1$ -LSP as this parameter enters only the Yukawa coupling of the $\tilde{\tau}_1$ and not the one of the $\tilde{\mu}_R$ (see figure 2.6). The lower limit for $\tan\beta$ is given by the LEP searches, which is why the plot starts at a value of 3.4 for $\tan\beta$ as anything lower than this has been excluded. For m_0 the $\tilde{\chi}_1^0$ is the candidate for the LSP at higher values of m_0 . As explained beforehand (Fig. 2.7), the ratio of $m_{1/2}$ to m_0 poses the upper limit for m_0 to allow for the $\tilde{\mu}_R$ -LSP, given a constant $m_{1/2}$. Note the NLSP switch from $\tilde{\tau}_1$ to $\tilde{\chi}_1^0$ marked by the dashed line.

One can see that the two dimensional histograms only allow for certain hierarchies between the LSP candidates. For variation of m_0 and $m_{1/2}$ (Fig. 2.7), with the other parameters set according to table 2.1, the hierarchy always alternates between the fairly rare

$$M_{\tilde{\mu}_R} < M_{\tilde{\chi}_1^0} < M_{\tilde{\tau}_1} \quad (2.1)$$

and the more often established

$$M_{\tilde{\chi}_1^0} < M_{\tilde{\mu}_R} < M_{\tilde{\tau}_1} \quad (2.2)$$

, as well as the following, most common scenario with the $\tilde{\mu}_R$ as the LSP, which is also the most often realized scenario for the histograms of A_0 against $m_{1/2}$ (Fig. 2.7) and m_0 against $\tan\beta$ (Fig. 2.9).

$$M_{\tilde{\mu}_R} < M_{\tilde{\tau}_1} < M_{\tilde{\chi}_1^0} \quad (2.3)$$

Note how these 3 hierarchies are the only ones to be realized in all the histograms. Another possible, but very seldom realized hierarchy is

$$M_{\tilde{\mu}_R} < M_{\tilde{\tau}_1} < M_{\tilde{e}_R} < M_{\tilde{\chi}_1^0} \quad (2.4)$$

, as this can only exist when the mass difference between the $\tilde{\mu}_R$ and the $\tilde{\chi}_1^0$ are fairly large. One possible configuration of parameters leading to this scenario is given in table 2.2.

m_0 in GeV	$m_{1/2}$ in GeV	A_0 in GeV	$\tan\beta$	$\text{sgn}\mu$
0	475	-1250	5	+

Table 2.2: Point in the B_3 mSUGRA parameter space leading to the hierarchy of equation 2.4, taken from H. K. Dreiner's publication [21]

The effect of the universal gaugino and scalar masses mostly allowing the configuration 2.3 and 2.2 is due to the nature of m_0 being the handle between gaugino and sfermion masses and $m_{1/2}$ basically influencing the entire spectrum. Thus both parameters shift many sparticle masses in a common direction, but only barely influence the hierarchy in between the sparticle masses they shift. Therefore the $\tilde{\mu}_R$ and $\tilde{\tau}_1$ masses have an almost constant and only fairly small difference for the variation of m_0 and $m_{1/2}$. Even though the region with $\tilde{\chi}_1^0$ expands towards lower values for the histograms involving A_0 (Fig. 2.8) and $\tan\beta$ (Fig. 2.9), the limits on the parameters exclude this configuration (Eq. 2.1) for the most part. These hierarchies of LSP, NLSP and NNLSP have a significant impact on the signatures that could be

discovered in colliders, which serves as the motivation for choosing a point in the parameter space to analyze in the next section.

2.2 Basic analysis of a point in the parameter space

As shown in the previous section, there are certain scenarios with different hierarchies of sparticle masses. Those scenarios have been quantified using the numeric calculations of `SOFTSUSY 3.1.7`. To give an impression of the lightest sparticles in each scenario, a benchmark point has been chosen for each individual case.

Parameter	Benchmark scenario		
	LM6	BP1	BP2
m_0	85	100	90
$m_{1/2}$	400	500	475
A_0	0	-1300	-1400
$\tan \beta$	10	4	4
$\text{sgn } \mu$	+	+	+
$\lambda_{132 GUT}$	0.0	0.045	0.045
Lightest sparticles (mass/GeV)			
LSP	$\tilde{\chi}_0^1$ (161.6)	$\tilde{\mu}_R$ (203.0)	$\tilde{\mu}_R$ (187.6)
NLSP	$\tilde{\tau}_1$ (170.7)	$\tilde{\chi}_0^1$ (206.6)	$\tilde{\tau}_1$ (194.3)
NNLSP	$\tilde{\mu}_R$ (178.18)	$\tilde{\tau}_1$ (208.6)	$\tilde{\chi}_0^1$ (195.9)
NNNLSP	\tilde{e}_R (178.19)	\tilde{e}_R (216.6)	\tilde{e}_R (204.1)

Table 2.3: Benchmark points (BP1 and BP2) in the B_3 mSUGRA parameter space in comparison to the LM6 of the CMS test points, with the corresponding 4 lightest sparticle masses. Each benchmark point has its characteristic hierarchy of the LSP to NNNLSP. All B_3 mSUGRA parameters are given at the GUT scale.

Table 2.3 shows the chosen benchmark points BP1 and BP2, as well as a mSUGRA test point from the CMS workgroup [48]. One can see the difference between the hierarchy and the masses of the lightest four sparticles. While both BP1 and BP2 favor a $\tilde{\mu}_R$ -LSP with either $\tilde{\tau}_1$ or the $\tilde{\chi}_0^1$ as the NLSP, LM6 features a different hierarchy with $\tilde{\chi}_0^1$ as the LSP, followed by $\tilde{\tau}_1$ and $\tilde{\mu}_R$. Aside from the specific hierarchies, the motivation to chose these points are the fairly low values of m_0 and $m_{1/2}$ so that early LHC research

data can be analyzed for signatures similar to the ones presented here. In particular the values of m_0 have been reduced by 10 GeV in comparison to the value of the two dimensional scans (Fig. 2.8 & 2.9). Only looking at m_0 and $m_{1/2}$, one can see that the mass spectrum is very dependent on these parameters. Minor differences lead to a ~ 20 GeV difference between LM6 and BP2 and also a ~ 15 GeV difference between BP2 and BP1. Shifting the focus on A_0 , one can see how the slepton masses are strongly influenced by the magnitude of the value of A_0 in combination with $\lambda_{132|GUT}$, being the heavier particles in LM6 in comparison to the lightest particle in BP2 and BP1. Note how the \tilde{e}_R remains the NNLSP in all scenarios as this specific LNV coupling does not enter the \tilde{e}_R 's mass evolution.

As BP2 has the most frequently seen configuration of sparticles, this is the benchmark point of choice for further analysis. As a next step, the calculated mass spectrum of SOFTSUSY 3.1.7 has been interfaced to ISAJET 7.64 to calculate the branching fractions. Table 2.4 shows the lower mass spectrum of all sparticles, as well as their decay channels and branching ratios. Taking these ratios into consideration, one can see that one of the major decay channels leads to a multi-lepton final state. It has this shape:

$$qq/gg \rightarrow \tilde{q}\tilde{q} \rightarrow jj\tilde{\chi}_0^1\tilde{\chi}_0^1 \rightarrow jj\mu\mu\tilde{\mu}_R\tilde{\mu}_R \quad (2.5)$$

Here \tilde{q} denotes a squark, whereas j is a jet and g a gluon. Starting with the decay channel of equation 2.5, the LHC signature will have the $\tilde{\mu}_R$ decaying into

$$\tilde{\mu}_R \rightarrow \begin{cases} e^-\nu_\tau \\ \tau^-\nu_e \end{cases} \quad (2.6)$$

and thus have the following form.

$$2j + 2\mu + \cancel{E}_T + \begin{cases} 2e^- \\ e^-\tau^- \\ 2\tau^- \end{cases} \quad (2.7)$$

This final state can be studied after feeding the input file provided by ISAJET 7.64 into HERWIG 6.510. Roughly 105 k events have been generated at $\sqrt{s} = 7$ TeV with CMS detector simulation to ensure sufficient statistics [49]. The parton distribution function (PDF) has been set to CTEQ6L. Note that the generated samples are only the signal itself without any specific background. To work with the generated ROOT-tuples ACSUSY has been employed.

Mass [GeV]	Channel	BR	Channel	BR
$\tilde{\mu}_R^-$	$\tau^- \nu_e$	50%	$e^- \nu_\tau$	50%
$\tilde{\tau}_1$	$\mu^- \bar{\nu}_e$	100%		
$\tilde{\chi}_1^0$	$\tilde{\mu}_R^- \mu^+$	50%	$\tilde{\mu}_R^+ \mu^-$	50%
\tilde{e}_R	$\tilde{\chi}_1^0 e^-$	100%		
$\tilde{\nu}_\tau$	$\tilde{\chi}_1^0 \nu_\tau$	70.1%	$W^+ \tilde{\tau}_1^-$	18%
	$e^+ \mu^-$	11.9%		
$\tilde{\nu}_e$	$\tilde{\chi}_1^0 \nu_e$	85.7%	$\tau^+ \mu^-$	14.3%
$\tilde{\nu}_\mu$	$\tilde{\chi}_1^0 \nu_\mu$	100%		
$\tilde{\tau}_2$	$\tilde{\chi}_1^0 \tau^-$	68.9%	$Z^0 \tilde{\tau}_1^-$	9%
	$H^0 \tilde{\tau}_1^-$	10.8%	$\mu^- \bar{\nu}_e$	11.3%
\tilde{e}_L^-	$\tilde{\chi}_1^0 e^-$	85.1%	$\mu^- \bar{\nu}_\tau$	14.9%
$\tilde{\mu}_L^-$	$\tilde{\chi}_1^0 \mu^-$	100%		
$\tilde{\chi}_2^0$	$\tilde{\chi}_1^0 H^0$	1.2%	$\tilde{e}_L^- e^+$	7.1%
	$\tilde{e}_L^+ e^-$	7.1%	$\tilde{\mu}_L^- \mu^+$	5.6%
	$\tilde{\mu}_L^+ \mu^-$	5.6%	$\tilde{\tau}_1^- \tau^+$	1.7%
	$\tilde{\tau}_1^+ \tau^-$	1.7%	$\tilde{\tau}_2^- \tau^+$	7.0%
	$\tilde{\tau}_2^+ \tau^-$	7.0%	$\tilde{\nu}_e \bar{\nu}_e$	9.6%
	$\tilde{\nu}_e^* \nu_e$	9.6%	$\tilde{\nu}_\mu \bar{\nu}_\mu$	7.9%
	$\tilde{\nu}_\mu^* \nu_\mu$	7.9%	$\tilde{\nu}_\tau \bar{\nu}_\tau$	10.3%
	$\tilde{\nu}_\tau^* \nu_\tau$	10.3%		
$\tilde{\chi}_1^-$	$\tilde{\chi}_1^0 W^-$	1.3%	$\tilde{\nu}_e e^-$	19.7%
	$\tilde{\nu}_\mu \mu^-$	16.2%	$\tilde{\nu}_\tau \tau^-$	21.3%
	$\tilde{e}_L^- \nu_e$	13.8%	$\tilde{\mu}_L^- \nu_\mu$	10.9%
	$\tilde{\tau}_1^- \nu_\tau$	3.3%	$\tilde{\tau}_2^- \nu_\tau$	13.5%
\tilde{t}_1	$\tilde{\chi}_1^0 t$	69.3%	$\tilde{\chi}_1^+ b$	30.7%
\tilde{b}_2	$\tilde{\chi}_2^0 b$	8.7%	$\tilde{\chi}_1^- t$	14.4%
	$W^- \tilde{t}_1$	76.4%		
\tilde{t}_2	$\tilde{\chi}_1^+ b$	14.9%	$Z^0 \tilde{t}_1$	51.2%
	$H^0 \tilde{t}_1$	26.5%	$\tilde{\chi}_1^0 t$	1.2%
	$\tilde{\chi}_2^0 t$	6.5%		
$\tilde{\chi}_3^0$	$\tilde{\chi}_1^+ W^-$	15.3%	$\tilde{\chi}_1^- W^+$	15.3%
	$\tilde{\chi}_1^0 Z^0$	4.0%	$\tilde{\chi}_2^0 Z^0$	13.9%
	$\tilde{t}_1 \tilde{t}$	24.8%	$\tilde{t}_1^* \tilde{t}$	24.8%
$\tilde{\chi}_2^-$	$\tilde{\chi}_1^0 W^+$	3.5%	$\tilde{\chi}_2^0 W^+$	14.0%
	$\tilde{t}_1 \tilde{b}$	54.1%	$\tilde{\chi}_1^- Z^0$	13.6%
	$\tilde{\chi}_1^- H^0$	12.9%		
$\tilde{\chi}_4^0$	$\tilde{\chi}_1^+ W^-$	10.4%	$\tilde{\chi}_1^- W^+$	10.4%
	$\tilde{\chi}_1^0 H^0$	2.6%	$\tilde{\chi}_2^0 H^0$	9.0%
	$\tilde{t}_1 \tilde{t}$	32.5%	$\tilde{t}_1^* \tilde{t}$	32.5%
\tilde{b}_1	$\tilde{\chi}_1^0 b$	69.6%	$\tilde{\chi}_1^+ t$	15.4%
	$W^- \tilde{t}_1$	24.7%	$H^0 \tilde{b}_1$	2.4%
$\tilde{u}_R / \tilde{c}_R$	$\tilde{\chi}_1^0 u / c$	100%		
$\tilde{d}_R / \tilde{s}_R$	$\tilde{\chi}_1^0 d / s$	100%		
$\tilde{d}_L / \tilde{s}_L$	$\tilde{\chi}_1^0 d / s$	1.6%	$\tilde{\chi}_2^0 d / s$	32.8%
	$\tilde{\chi}_1^- u / c$	65.6%		

	Mass [GeV]	Channel	BR	Channel	BR
\tilde{u}_L/\tilde{c}_L	1007.7	$\tilde{\chi}_1^0 u/c$	1.2%	$\tilde{\chi}_2^0 u/c$	33.0%
		$\tilde{\chi}_1^+ d/s$	65.8%		
\tilde{g}	1093.3	$\tilde{u}_L^* u$	1.2%	$\tilde{u}_L \bar{u}$	1.2%
		$\tilde{d}_L^* d$	1.1%	$\tilde{d}_L \bar{d}$	1.1%
		$\tilde{u}_R^* u$	2.3%	$\tilde{u}_R \bar{u}$	2.3%
		$\tilde{d}_R^* d$	2.4%	$\tilde{d}_R \bar{d}$	2.4%
		$\tilde{s}_L^* s$	1.1%	$\tilde{s}_L \bar{s}$	1.1%
		$\tilde{s}_R^* s$	2.4%	$\tilde{s}_R \bar{s}$	2.4%
		$\tilde{c}_L^* c$	1.2%	$\tilde{c}_L \bar{c}$	1.2%
		$\tilde{c}_R^* c$	2.3%	$\tilde{c}_R \bar{c}$	2.3%
		$\tilde{b}_1^* b$	8.5%	$\tilde{b}_1 \bar{b}$	8.5%
		$\tilde{b}_2^* b$	2.5%	$\tilde{b}_2 \bar{b}$	2.5%
		$\tilde{t}_1^* t$	22.2%	$\tilde{t}_1 \bar{t}$	22.2%
		$\tilde{t}_2^* t$	2.8%	$\tilde{t}_2 \bar{t}$	2.8%

Table 2.4: Lower mass spectrum relevant for $\tilde{\mu}_R$ -LSP decay with the respective branching ratios (BR) of BP2 (Tab. 2.3). The mass spectrum is given by SOFTSUSY 3.1.7, whereas the branching ratios are provided by ISAJET 7.64. Branching ratios lower than 1% have been neglected.

This software has been developed by our institute and elegantly enables the user to loop over and analyze the aforementioned ROOT-tuples event by event. It also has integrated ROOT support which will be used to provide the particle attribute distributions in the form of histograms.

Object selection criteria The selection criteria differs for all objects in the final state (Eq. 2.7). For muons the absolute value of the pseudorapidity $|\eta|$ has to be smaller than 2.1, as this is where the CMS detector efficiency drops rapidly due to the limited space covered by the tracker. The muon track isolation is not allowed to exceed 3 GeV. The normalized χ^2 value of the tracker has to be lower than 10 and the absolute value of the impact parameter $|d_0|$ for the inner track has to be lower than 0.2. The minimal amount of hits has been set to 11 while the valid pixel and muon chamber hits have to be at least equal to 1 and the number of matched chambers needs to be 2 or larger. The muon is also required to be a global muon. As we have a fairly low mass difference between the $\tilde{\chi}_1^0$ and the $\tilde{\mu}_R$ the transversal momentum only has to be larger than $p_T > 10$ GeV.

For electrons the selection criteria have been taken from the CERN Twiki page [50]. The values of the WP90 cuts have been chosen for a 90% efficiency. The selection has also been split into barrel and endcaps using the $|\eta|$ values and been handled separately. The first section of the table for the WP90 cuts concerning the electron-positron pair production, titled ‘‘Conversion Re-

jection”, has been skipped because they are too hard. As an additional requirement for selection the E_T has to be larger than 10 GeV. Note that the E_T has been chosen for electrons because of the more precise measurement in the electromagnetic calorimeter in comparison to the p_T measurement in the tracker. Because tau leptons have not been implemented in the software version that is being used, they are being neglected. This of course disfavors the analysis of the third scenario in the final state (Eq. 2.7).

For the jet selection the particle flow algorithm has been chosen. Here an absolute value of $|\eta| < 2.4$ in combination with a minimum transversal momentum of 30 GeV are the criteria for their selection. There also have to be at least more than a single constituent in each jet. For the comparison of the shapes of the distributions the generated p_T of the u , d , s , c and t quarks has been extracted as well. Here the requirements for selection have been $p_T > 30$ GeV for both the u , d , s and c quarks as well as the t quark to match the jet p_T criteria.

Characterization of the final state As the final state (Eq. 2.7) is being characterized by its components and their distributions, they will be studied after extracting them using the object selection criteria. The process has a cross section of $\sigma = 0.1056$ pb with a total number of events of $N = 104911$. Using those values all distributions have been normalized to an integrated luminosity of $\int \mathcal{L} dt = 10 \text{ fb}^{-1}$. As shown in figure 2.10a, the muons tend to be very soft. This is the case because most of them stem from the decay of the $\tilde{\chi}_1^0 \rightarrow \tilde{\mu}_R \mu$, with only a relatively small mass difference between both supersymmetric particles. One may reach a point where the standard cuts for the muon p_T at CMS research might prevent finding these signatures. Comparing the generated and detected muon p_T , one can see that the shape of the distribution is almost identical, meaning that the chosen selection criteria fits the scenario quite well. The amount of the generated muons peaks around 6 GeV, but is still fairly close the number of selected muons at the cut off value of $p_T > 10$ GeV. For the selected electron E_T the shape of the distribution is also similar to the one of the generated electrons upwards of 50 GeV. Below that threshold the amount of selected electrons drops quickly while the generated ones rise to an significantly higher amount, especially below 10 GeV. This difference is due to the isolation requirements of the WP90 selection criteria, as they cut out a lot of the pair production and electrons from jets. Most of the selected electrons are significantly harder than the muons due to the decay channel $\tilde{\mu}_R \rightarrow e^- \nu_\tau$ allowing for a larger amount of energy being available to the electrons. Amongst all the soft muons, the hardest muons (Fig. 2.11a & 2.11b), the ones that are most

likely to stem from the supersymmetric decay, show a similar distribution with a tendency towards energies below 30 GeV.

The hardest jets on the other hand, have quite large values of p_T with noticeable differences between the hardest (Fig. 2.12a) and second hardest jet (Fig. 2.12b). While the p_T of the hardest jet peaks around 130 GeV and 440 GeV, the p_T of the second hardest jet only peaks around 110 GeV with a spread out bump in the region between 220 GeV to 440 GeV. The additional distributions show the p_T of t as well as u , d , s and c quarks, that *only* stem from a squark decay. These distributions are the main source for the peaks in the jet p_T spectrum. The peak around the 130 GeV region stems mostly from the $\tilde{t}_1 \rightarrow \tilde{\chi}_1^0 t$ decay and the peak in the 440 GeV region is mostly the result of the decay of the first and second generation squarks into the $\tilde{c}\tilde{h}_1^0$ and the respective quark of the same generation. Note however that these p_T distributions of the quarks are only shown for comparison and are not the only constituents of the jets. This can be seen in figure 2.12a, where the tail of the first and second generation quarks' distribution drops below the jet p_T distribution.

The selected number of electrons and muons added up (Fig. 2.13b) and the number of muons separately (Fig. 2.13a) both resemble their generated counterparts. The distributions are of course shifted towards the left as some leptons are rejected by the object selection and therefore less particles remain overall. The peak for the selected muons is at 1, while the peak of all selected leptons (μ, e) is at 2. Since the width of the peaks is quite high, the necessary amount of 2 muons and the necessary amount of 3 leptons still have similar amounts of counted events as they are very close to the peak. The minimal amount of 2 muons and 3 leptons (μ, e) stems from the composition of the final state (Eq. 2.7), where the 3 leptons (μ, e) are the result of taking the average of the 3 equiprobable decay channels and adding the 2 muons. τ leptons are not included. Demanding an overall amount of 3 leptons (μ, e) for each event leads to an efficiency of $45373/104911 \approx 43\%$.

Applying this requirement of at least 3 leptons (μ, e) onto the number of jets (Fig. 2.14a) and the \cancel{E}_T distribution (Fig 2.14b) shows the efficiency. One can see a significant drop in the amount of events for each bin, though the shape of the distribution has been retained. Contrary to the number of leptons (μ, e), the peak of the jet distribution is at 3 while we only need at least 2 jets for the final state (Eq. 2.7). The quite large amount of missing transversal energy is due to the neutrino production at the decay of the $\tilde{\mu}_R$. For R-parity conserving cases the lightest neutralino $\tilde{\chi}_1^0$ usually is a stable particle and will escape detection due its electric charge being equal to 0. It is heavier than neutralinos and the \cancel{E}_T distribution would therefore have a

higher peak at lower energies, but would drop faster towards higher energies. Neutrinos provide a distribution with a lower peak, but a smoother tail as shown by figure 2.14b.

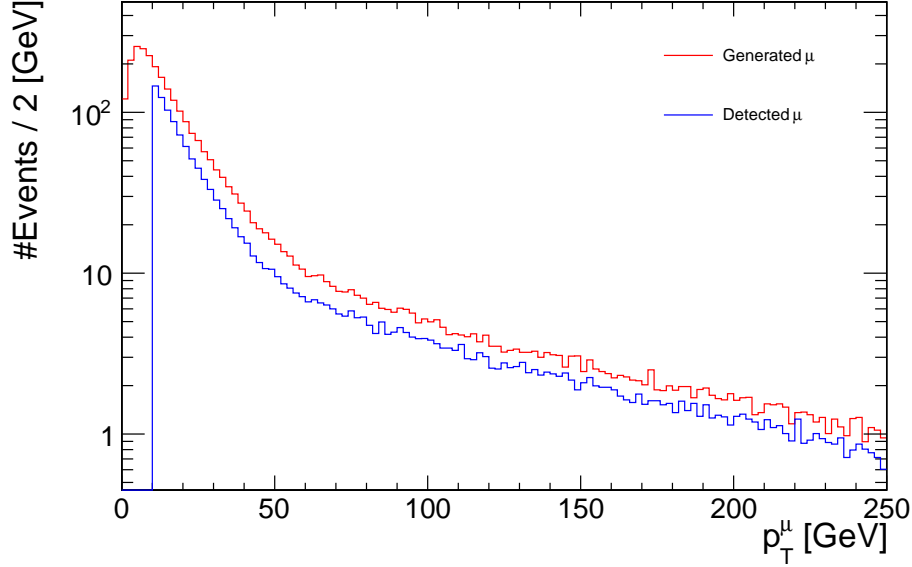
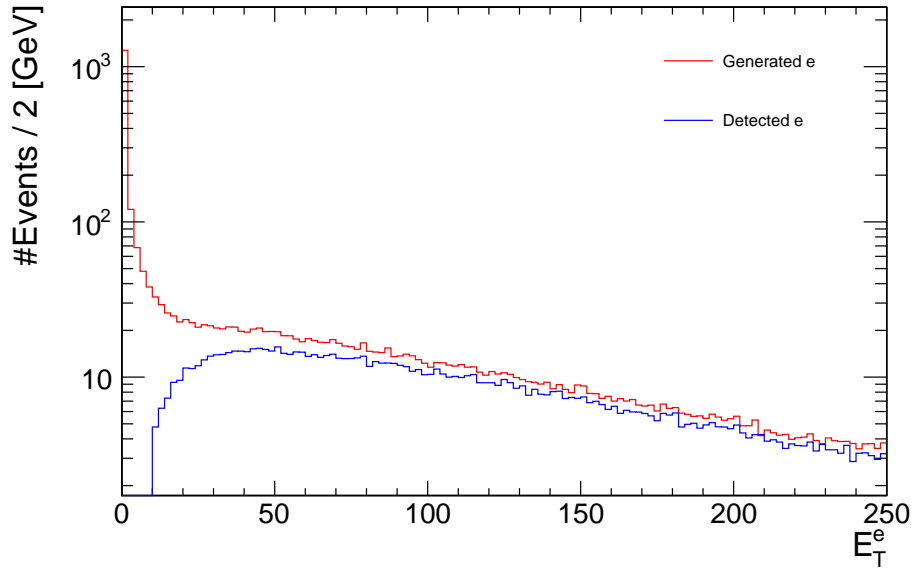

 (a) p_T of all selected and all generated muons

 (b) E_T of all selected and all generated electrons

Figure 2.10: Generated and selected muon p_T (Fig. 2.10a) and electron E_T (Fig. 2.10b) distributions in the B_3 mSUGRA benchmark model BP2 (Tab. 2.3). The distributions are normalized to an integrated luminosity of $\int \mathcal{L} dt = 10 \text{ fb}^{-1}$.

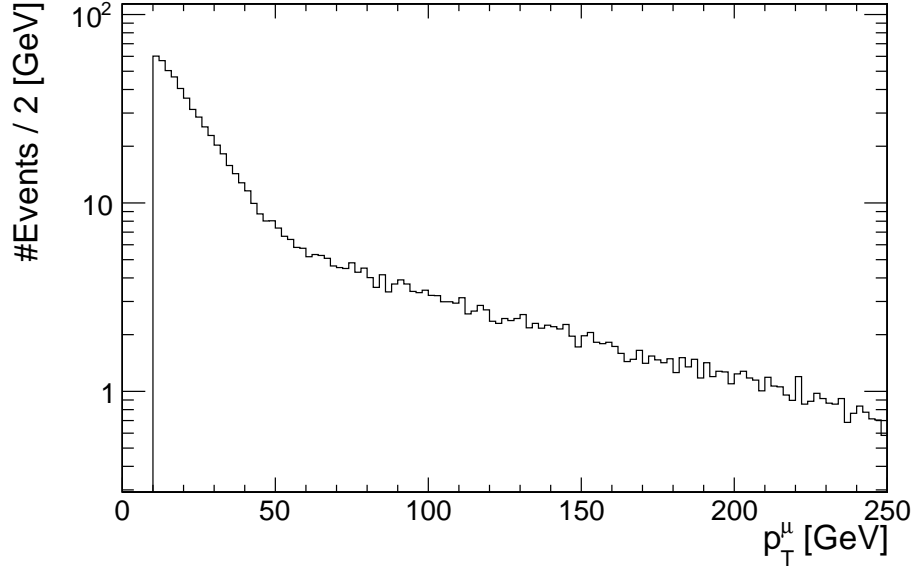
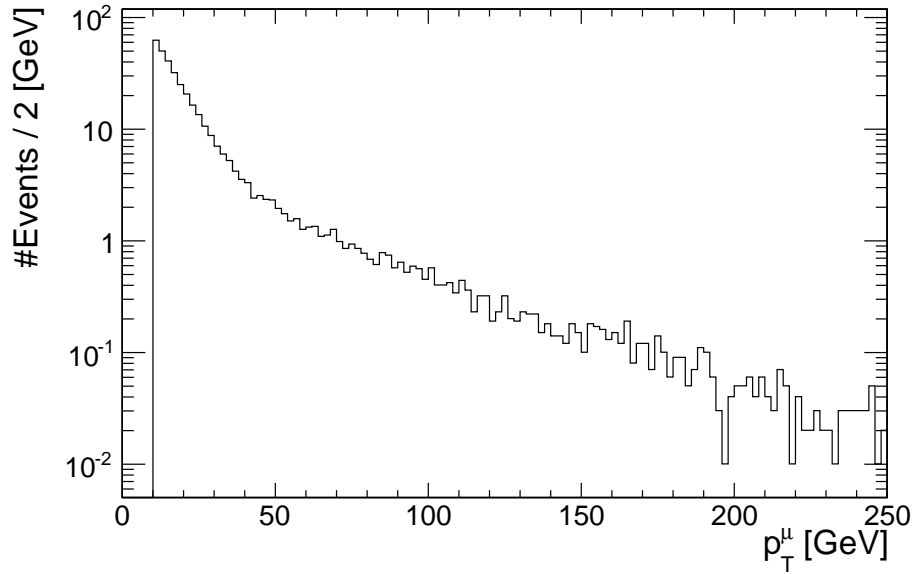
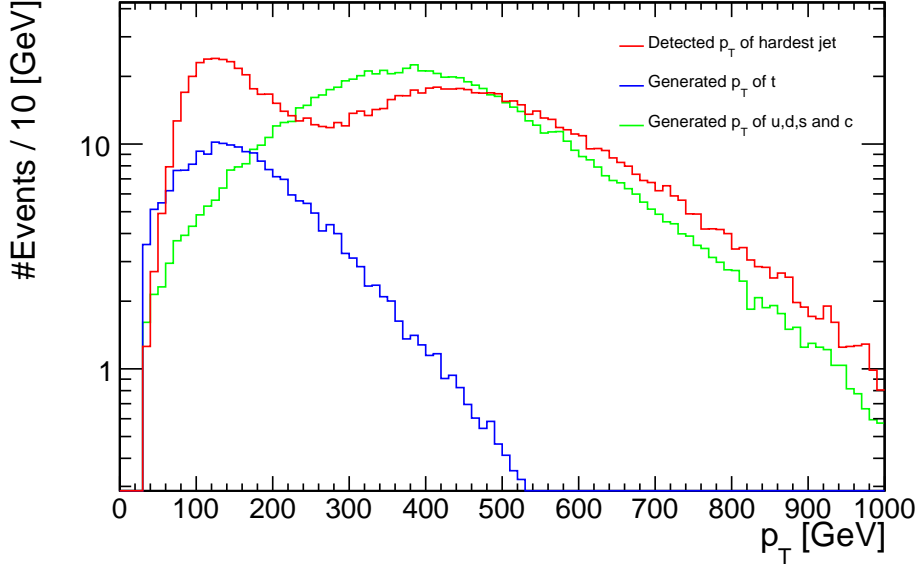
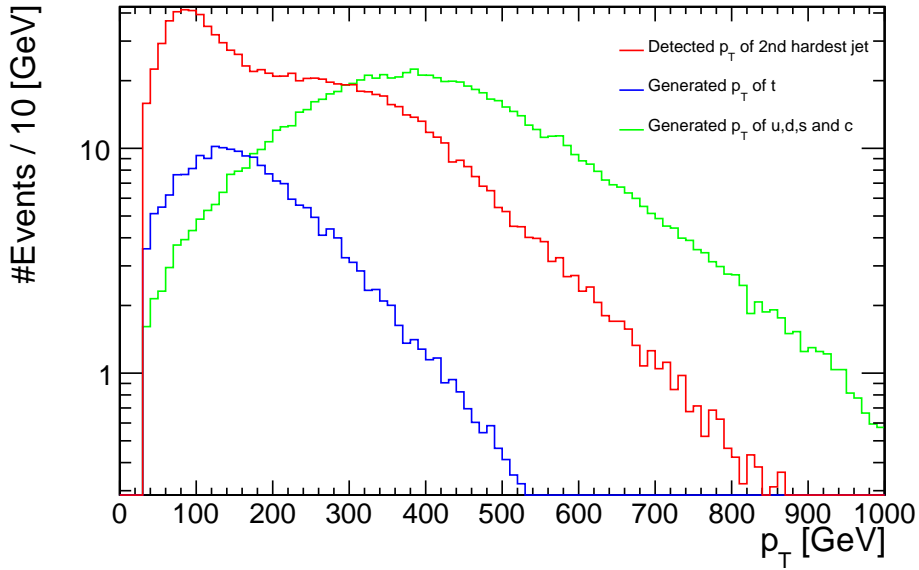
(a) p_T of the hardest muon(b) p_T of the second hardest muon

Figure 2.11: p_T distributions of the first (Fig. 2.11a) and second hardest muon (Fig. 2.11b) of each event in the B_3 mSUGRA benchmark model BP2 (Tab. 2.3). The distributions are normalized to an integrated luminosity of $\int \mathcal{L} dt = 10 \text{ fb}^{-1}$.

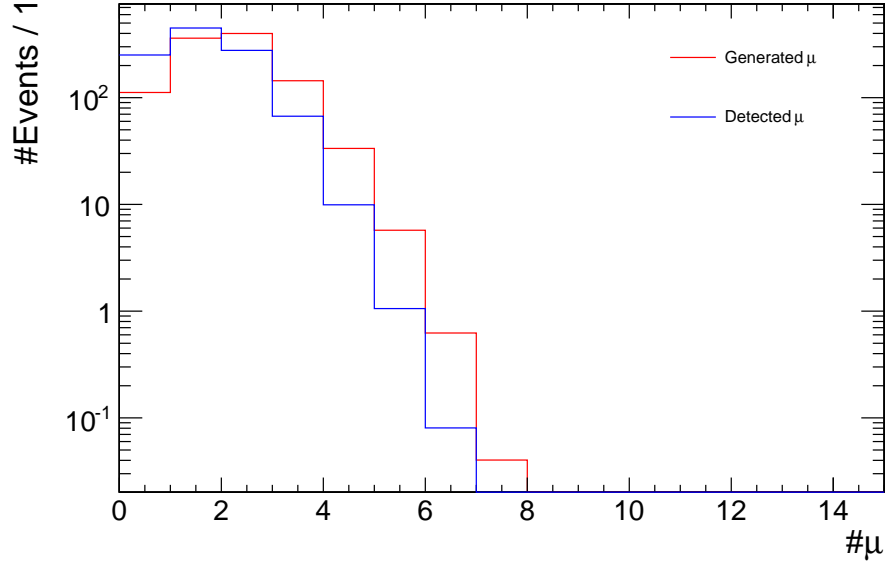


(a) p_T of the hardest jet as well as the p_T of u , d , s , c that originate from first and second generation squark decays and t quarks that originate from \tilde{t}_1 decays

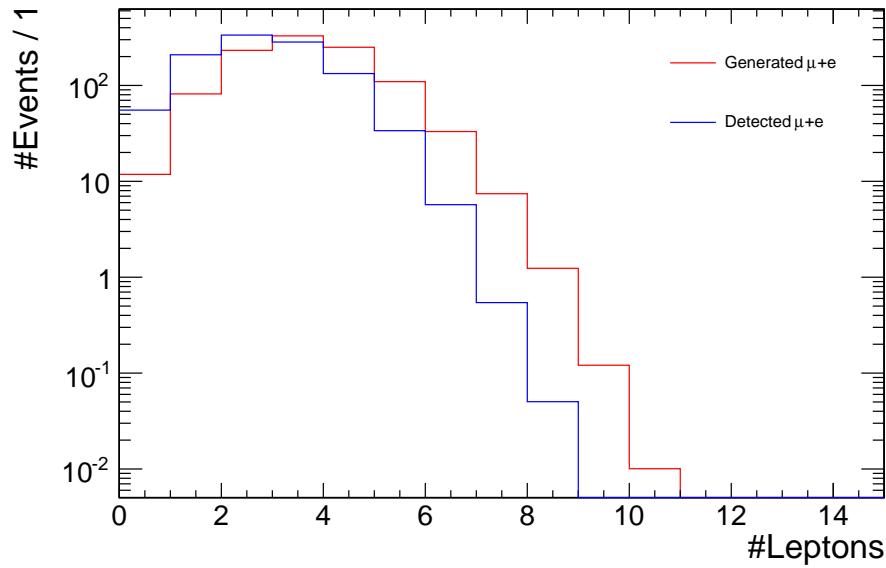


(b) p_T of the 2nd hardest jet as well as the p_T of u , d , s , c that originate from first and second generation squark decays and t quarks that originate from \tilde{t}_1 decays

Figure 2.12: p_T distributions of the hardest jet (Fig. 2.12a), second hardest jet (Fig. 2.12b) and quarks that stem from first and second generation squark and \tilde{t}_1 decays, respectively, of each event in the B_3 mSUGRA benchmark model BP2 (Tab. 2.3). The distributions are normalized to an integrated luminosity of $\int \mathcal{L} dt = 10 \text{ fb}^{-1}$.



(a) Generated number of muons in red and selected number of muons in blue



(b) Generated number of muon plus electrons in red and selected number of muons+electrons in blue

Figure 2.13: Distributions of the number of generated and selected muons (Fig. 2.14a) and leptons (Fig. 2.13b) in the B₃ mSUGRA benchmark model BP2 (Tab. 2.3). The distributions are normalized to an integrated luminosity of $\int \mathcal{L} dt = 10 \text{ fb}^{-1}$.

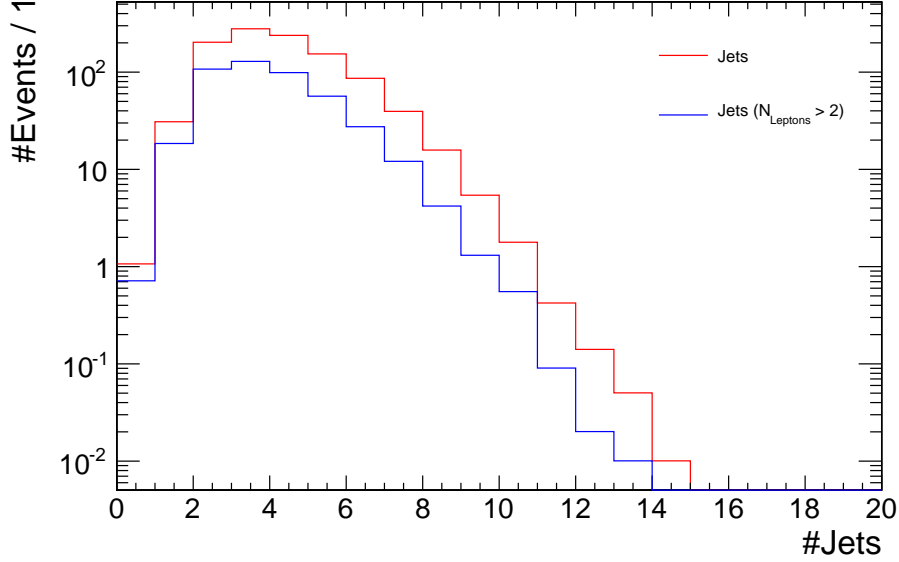
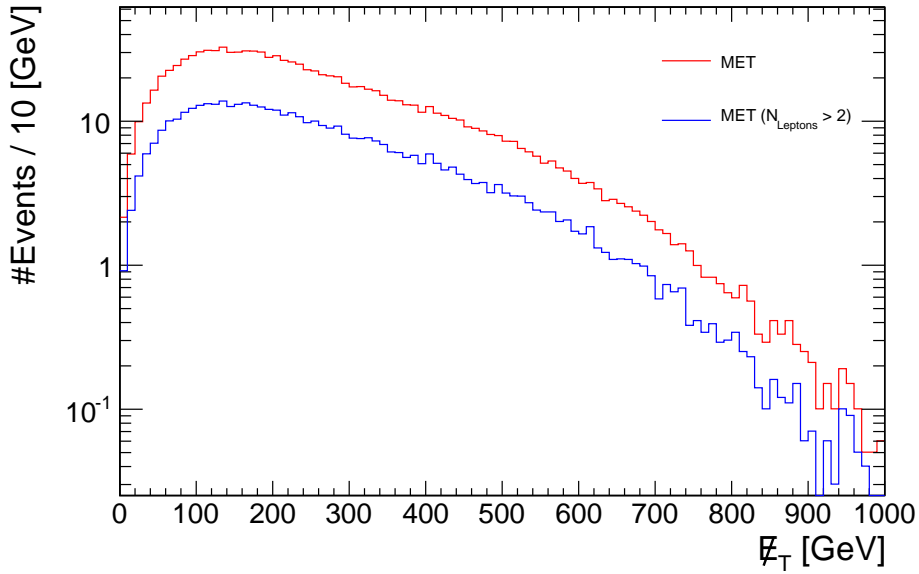

 (a) #jets in red and #jets in an event with more than 2 leptons (μ, e) in blue

 (b) E_T distribution with and without more than 3 leptons (μ, e)

Figure 2.14: Number of jets and E_T distributions with and without a minimum of 3 leptons (μ, e) in the B_3 mSUGRA benchmark model BP2 (Tab. 2.3). The distributions are normalized to an integrated luminosity of $\int \mathcal{L} dt = 10 \text{ fb}^{-1}$.

2.3 Conclusion

As a conclusion one can see that the B_3 mSUGRA parameter space with the $\tilde{\mu}_R$ -LSP is very limited, but judging from the cross section $\sigma = 0.1056$ pb, is still worth looking for.

For searching the $\tilde{\mu}_R$ -LSP at the LHC, the universal gaugino mass $m_{1/2}$ can range between 400 GeV and 1400 GeV. These bounds allow the universal scalar mass m_0 to be in between 0 GeV and 600 GeV. The ratio of $m_{1/2}$ to m_0 has to be approximately greater than 4 for values of $m_{1/2}$ higher than 130 GeV. Below that the ratio rises, but not linearly. The universal trilinear scalar coupling strength A_0 should be negative to allow for lower masses of the $\tilde{\mu}_R$ and needs to be of high magnitude to allow for low $m_{1/2}$. The tangents of the ratio of the two Higgs vacuum expectation values $\tan\beta$ is limited to a range of 3.4 to around 5.6. The upper bound can vary depending on the other parameters, but anything above 10 can be excluded for the current state of the LHC. Towards the maximum capacity of the LHC, meaning for high $m_{1/2}$, the upper bound of $\tan\beta$ can rise towards 20. The sign of the bilinear Higgs mixing parameter needs to be positive, otherwise it limits the range of $\tan\beta$ even further.

It has been shown that the mass hierarchy

$$M_{\tilde{\mu}_R} < M_{\tilde{\tau}_1} < M_{\tilde{\chi}_1^0}$$

is the most dominant one with the $\tilde{\mu}_R$ -LSP. Analyzing a specific point in the parameter space featuring this hierarchy has shown that one of the major decay channels is

$$qq/gg \rightarrow \tilde{q}\tilde{q} \rightarrow jj\tilde{\chi}_0^1\tilde{\chi}_0^1 \rightarrow jj\mu\mu\tilde{\mu}_R\tilde{\mu}_R$$

which leads to a final state with the following composition.

$$2j + 2\mu + \cancel{E}_T + \begin{cases} 2e^- \\ e^-\tau^- \\ 2\tau^- \end{cases}$$

Event generation has given insight into various distributions of the final state components of the simulated signal. One has seen that the transversal momentum of the muons tends to be low, while the electrons have a higher p_T spectrum due to the mass differences of the respective decay channel's particles. The hardest muons' had a similar p_T distribution to the one of all selected muons. The shape of the hardest jet transversal momentum distributions have shown information that the first and second generation

squark as well as the \tilde{t}_1 decay channel lead to characteristic peaks. The number of leptons (μ, e) and muons illustrated the efficiency of 43% for the minimal amount of 3 leptons. This requirement has then been tested on the \cancel{E}_T distribution and the number of jets. Aside from less selected entries overall, no significant change in shape has been noted. These distributions should be kept in mind when scanning data for similar points in the B_3 mSUGRA parameter space.

Further studies on the used benchmark point with standard model background should be the next step. They are required to estimate the effect on the distributions and whether the selection criteria is still sufficient to isolate the supersymmetric processes.

Bibliography

- [1] P.J. Mohr, B.N. Taylor (2005), "[CODATA recommended values of the fundamental physical constants: 2002](#)", *Reviews of Modern Physics* **77**: 1–107. Bibcode [2005RvMP...77....1M](#), doi:[10.1103/RevModPhys.77.1](#), An in-depth discussion of how the CODATA constants were selected and determined.
- [2] A. Salam and J.C. Ward, *Gauge Theory of Elementary Interactions*, *Phys. Rev. B* **763** (1964) 136, http://prola.aps.org/abstract/PR/v136/i3B/pB763_1.
- [3] S. Weinberg, *A Model of Leptons*, *Phys. Rev. Lett.* **19** (1967) 1264, http://prola.aps.org/abstract/PRL/v19/i21/p1264_1.
- [4] S.L. Glashow, J. Iliopoulos, and L. Maiani, *Weak Interactions with Lepton-Hadron Symmetry*, *Phys. Rev. D* **2** (1970) 1285 , http://prola.aps.org/abstract/PRD/v2/i7/p1285_1.
- [5] F. Halzen and A.D. Martin, *Quarks and Leptons: An introduction course in modern particle physics*, John Wiley & Sons, 1984. ISBN 0-471-88741-2.
- [6] Fehling, Dave. [The Standard Model of Particle Physics: A Lunchbox's Guide](#), The Johns Hopkins University, Retrieved on 2008-12-03.
- [7] H. P. Nilles, *Supersymmetry, supergravity and particle physics*, *Phys. Rept.* **110** (1984), 1;
- [8] H. E. Haber and G. L. Kane, *The search for supersymmetry: Probing physics beyond the standard model*, *Phys. Rept.* **117** (1985), 75.
- [9] M. Drees, *An introduction to supersymmetry* (1996), APCTP-5 KEK-TH-501, arXiv:[hep-ph/9611409](#).

-
- [10] *A Supersymmetry primer*, Stephen P. Martin, (Michigan U.) . Sep 1997. 88pp, In *Kane, G.L. (ed.): Perspectives on supersymmetry II* 1-153, e-Print: [hep-ph/9709356](https://arxiv.org/abs/hep-ph/9709356).
- [11] S. Dimopoulos, H. Georgi (1981), "Softly Broken Supersymmetry and SU(5)", Nuclear Physics B **193**: 150, Bibcode [1981NuPhB.193..150D](https://arxiv.org/abs/1981NuPhB.193..150D), doi:[10.1016/0550-3213\(81\)90522-8](https://doi.org/10.1016/0550-3213(81)90522-8).
- [12] S. Dimopoulos, S. Raby and F. Wilczek, Phys. Lett. B **112** (1982) 133.
- [13] A. Y. Smirnov and F. Vissani, Physik. Lett. B **380** (1996) 317, arXiv:[hep-ph/9601387v1](https://arxiv.org/abs/hep-ph/9601387v1).
- [14] G. Bhattacharyya and P. B. Pal, Phys. Rev. D **59** (1999) 097701, arXiv:[hep-ph/9601387](https://arxiv.org/abs/hep-ph/9601387).
- [15] L. E. Ibanez and G. G. Ross, Phys. Lett. B **260** (1991) 291.
- [16] L. E. Ibanez and G. G. Ross, Phys. Lett. B **368** (1992) 3.
- [17] H. K. Dreiner, C. Luhn and M. Thormeier, Phys. Rev. D **73** (2006) 075007, arXiv:[hep-ph/0512163](https://arxiv.org/abs/hep-ph/0512163).
- [18] P. van Nieuwenhuizen, Phys. Rep. 68, **189** (1981)
- [19] B. C. Allanach, A. Dedes, H. K. Dreiner, Phys. Rev. **D69** (2004) 115002, arXiv:[hep-ph/0309196](https://arxiv.org/abs/hep-ph/0309196).
- [20] B. C. Allanach, M. A. Bernhardt, H. K. Dreiner *et al.*, Phys Rev. **D75** (2007) 035002, arXiv:[hep-ph/0609263](https://arxiv.org/abs/hep-ph/0609263).
- [21] H.K. Dreiner, (Bonn U.) , S. Grab, (UC, Santa Cruz) , T. Stefaniak, (Bonn U. & Gottingen U., II. Phys. Inst.), BONN-TH-2011-04, SCIPP-11-01, Feb 2011. 33pp, e-Print: [hep-ph/1102.3189](https://arxiv.org/abs/hep-ph/1102.3189) [hep-ph].
- [22] R. Barbieri, F. Caravaglios, M. Frigeni and M. L. Mangano, Nucl. Physik. B **367** (1991) 28.
- [23] K. Desch, H. K. Dreiner, S. Fleischmann, S. Grab and P. Wienemann, Phys. Rev. D **83** (2011) 015013, arXiv: [hep-ph/1008.1580](https://arxiv.org/abs/hep-ph/1008.1580) [hep-ph].
- [24] G. Aad *et al.* [ATLAS Collaboration], arXiv: [hep-ph/0901.0512](https://arxiv.org/abs/hep-ph/0901.0512) [hep-ex].
- [25] H. K. Dreiner, C. Luhn, H. Murayama *et al.*, Nucl. Phys. **B774** (2007) 127-167, [[hep-ph/0610026](https://arxiv.org/abs/hep-ph/0610026)].

-
- [26] H. K. Dreiner, arXiv:[hep-ph/9707435](https://arxiv.org/abs/hep-ph/9707435).
- [27] H. K. Dreiner, S. Grab and M. K. Trenkel, Phys. Rev. D **79** (2009) 016002 [Erratum-ibid. **79** (2009) 019902] [arXiv:[hep-ph/0207334](https://arxiv.org/abs/hep-ph/0207334)].
- [28] B. C. Allanch, A. Dedes and H. K. Dreiner, Phys. Rev. D **60**, 056002 (1999) [arXiv:[hep-ph/9902251](https://arxiv.org/abs/hep-ph/9902251)].
- [29] B. de Carlos and P. L. White, Phys. Rev. D **54** (1996) 3427 [arXiv:[hep-ph/9602381](https://arxiv.org/abs/hep-ph/9602381)].
- [30] S. Abdullin, Z. Antunovic, F. Charles, M. Dzelalija, CMS Note 1999/018.
- [31] R. Barate *et al.* [LEP Working Group for Higgs boson searches and ALEPH Collaboration and and], Phys. Lett. B **565** (2003) 61, arXiv:[hep-ex/0306033](https://arxiv.org/abs/hep-ex/0306033).
- [32] S. Schael *et al.* [ALEPH Collaboration and DELPHI Collaboration and L3 Collaboration and], Eur. Phys. J. C **47** (2006) 547, arXiv:[hep-ex/0602042](https://arxiv.org/abs/hep-ex/0602042).
- [33] LEPSUSYWG, ALEPH, DELPHI, L3 and OPAL experiments, note LEPSUSYWG/04-07.1, http://lepsusy.web.cern.ch/lepsusy/www/lsp_cmssm_summer04/cMSSM_final.html
- [34] ALEPH Collaboration, Absolute mass lower limit for the lightest neutralino of the MSSM from e^+e^- data at \sqrt{s} up to 209 GeV, Phys. Lett. B **583** (2004) 247.
- [35] BABAR Collaboration, B. Aubert, et al, BABAR-PUB-09/018, SLAC-PUB-13846, arXiv:[0912.0242v2](https://arxiv.org/abs/0912.0242v2) [hep-ex].
- [36] K. Nakamura et al. (Particle Data Group), J. Phys. G **37**, 075021 (2010) and 2011 partial update for the 2012 edition.
- [37] B.C. Allanach, Comput. Phys. Commun. **143** (2002) 305-331, arXiv:[hep-ph/0104145](https://arxiv.org/abs/hep-ph/0104145)
- [38] B.C. Allanach and M.A. Bernhardt, Comput. Phys. Commun. **181** (2010) 232, arXiv:[0903.1805](https://arxiv.org/abs/0903.1805).
- [39] HERWIG 6.5, G. Corcella, I.G. Knowles, G. Marchesini, S. Moretti, K. Odagiri, P. Richardson, M.H. Seymour and B.R. Webber, JHEP 0101 (2001) 010 [[hep-ph/0011363](https://arxiv.org/abs/hep-ph/0011363)]; [hep-ph/0210213](https://arxiv.org/abs/hep-ph/0210213).

-
- [40] S. Moretti, K. Odagiri, P. Richardson, M.H. Seymour and B.R. Webber, JHEP 0204 (2002) 028 [[hep-ph/0204123](#)].
- [41] F. E. Paige, S. D. Protopopescu, H. Baer and X. Tata, arXiv:[hep-ph/0312045](#).
- [42] CMS Physics Technical Design Report, Vol.II, Physics Performance, CERN/LHCC 06-021, CMS TDR 8.2.
- [43] M. Drees and S. P. Martin, arXiv:[hep-ph/9504324](#).
- [44] L. E. Ibanez, C. Lopez and C. Munoz, Nucl. Phys. B **256** (1985) 218.
- [45] B. C. Allanach, S. Kraml and W. Porod, JHEP **0303** (2003) 016, arXiv:[hep-ph/0302102](#).
- [46] G. Degrassi, S. Heinemeyer, W. Hollik, P. Slavich and G. Weiglein, Eur. Phys. J. C **28** (2003) 133, arXiv:[hep-ph/0212020](#)
- [47] B. C. Allanach, A. Djouadi, J. L. Kneur, W. Porod and P. Slavich, JHEP **0409** (2004) 044, arXiv:[hep-ph/0406166](#)
- [48] CMS Physics Technical Design Report, Vol.II, Physics Performance, CERN/LHCC 06-021, CMS TDR 8.2
- [49] Lars Sonnenschein, Private communications (2011), Herwig event generation.
- [50] WP Cuts on electrons,
<https://twiki.cern.ch/twiki/bin/viewauth/CMS/SimpleCutBasedEleID>

2.4 Acknowledgements

First of all I would like to thank Prof. Thomas Hebbeker for enabling me to write this thesis at the institute of physics III A of the RWTH Aachen. It has been a very interesting topic to research and has been set up rather spontaneously during private discussions with Arnd Meyer and Carsten Magass.

Carsten Magass was a great help in setting up and getting to know Linux and C++. He certainly saved me from spending a lot of time on getting my programming environment set up properly.

Furthermore I would also like to thank all my co-workers at the institute for their advice, especially my officemates Metin Ata and Andreas GÜth. Without their everyday assistance, the task would have been way more time consuming and probably close to impossible.

Deborah Duchardt and Matthias Endres introduced me to supersymmetry and also helped me to get to know the ACSUSY framework. Especially the first part was detrimental as my thesis' is based on supersymmetry. Our discussions were very helpful and enjoyable overall.

In particular I would like to thank Arnd Meyer for his guidance throughout my studies and Lars Sonnenschein for helping me to set up the applications and generating the events.

The overall atmosphere was very pleasing to live and work in. Once again I would like to thank all my colleagues for that.